CHEMISTRY
AN ASIAN JOURNAL

DOI: 10.1002/asia.200800226

Phosphorescence Color Tuning by Ligand, and Substituent Effects of Multifunctional Iridium(III) Cyclometalates with 9-Arylcarbazole Moieties

Cheuk-Lam Ho,[a] Qi Wang,[c] Ching-Shan Lam,[a] Wai-Yeung Wong,*[a, b] Dongge Ma,*[c] Lixiang Wang,[c] Zhi-Qiang Gao,[b] Chin-Hsin Chen,[b] Kok-Wai Cheah,[b] and Zhenyang Lin[d]

Abstract: The synthesis, isomeric studies, and photophysical characterization of a series of multifunctional cyclometalated iridium(III) complexes containing a fluoro- or methyl-substituted 2-[3-(*N*-phenylcarbazolyl)]pyridine molecular framework are presented. All of the complexes are thermally stable solids and highly efficient electrophosphors. The optical, electrochemical, photo-, and electrophosphorescence traits of these iridium phosphors have been studied in terms of the electronic nature and coordinating site of the aryl or pyridyl ring substituents. The correlation between the functional properties of these phosphors and the results of density functional theory calculations was made. Arising from the propensity of the electron-rich carbazolyl group to facilitate hole injection/transport, the presence of such a moiety can increase the highest-occupied molecular orbital levels and improve the charge balance in the resulting complexes relative to the parent phosphor with 2-phenylpyridine ligands. Remarkably, the excited-state properties can be manipulated through ligand and substituent effects that allow the tuning of phosphorescence energies from bluish green to deep red. Electrophosphorescent organic light-emitting diodes (OLEDs) with outstanding device performance can be fabricated based on these materials, which show a maximum current efficiency of approximately 43.4 cd A^{-1}, corresponding to an external quantum efficiency of approximately 12.9% ph/el (photons per electron) and a power efficiency of approximately 33.4 Lm W^{-1} for the best device. The present work provides a new avenue for the rational design of multifunctional iridium–carbazolyl electrophosphors, by synthetically tailoring the carbazolyl pyridine ring that can reveal a superior device performance coupled with good color-tuning versatility, suitable for multicolor-display technology.

Keywords: carbazole · color tuning · iridium complexes · organic light-emitting diodes · phosphorescence

Introduction

Organic light-emitting diodes (OLEDs) attract considerable attention for applications in multicolor displays and lighting applications.[1] In OLEDs, visible light is generated by radiative decay of excited states formed by the recombination of holes and electrons injected into the organic semiconductor.[2] Spin statistics favor the formation of triplet over singlet excited states, which poses a limitation to the internal quantum efficiency of OLEDs based on fluorescent small molecules or polymers ($\leq$25%).[3] By using phosphorescent emitters in the active layer, it is possible to capture both singlet and triplet excited states and increase the internal quantum efficiency as high as 100%.[4] In recent years, considerable progress in electrophosphorescent OLEDs has been achieved by using organometallic complexes as dopants in small organic hosts.[4c,5] Along this line of frontier science, iridium(III) complexes functionalized with orthometalated ligands (CN) constitute one of the most important paradigms of the device configuration. The large spin–orbit coupling associated with the iridium(III) ion causes the triplet metal-to-

[a] Dr. C.-L. Ho, C.-S. Lam, Prof. W.-Y. Wong
Department of Chemistry
Hong Kong Baptist University
Waterloo Road, Kowloon Tong, Hong Kong (P.R. China)
Fax: (+86) 852-3411-7348
E-mail: rwywong@hkbu.edu.hk

[b] Prof. W.-Y. Wong, Dr. Z.-Q. Gao, Prof. C.-H. Chen, Prof. K.-W. Cheah
Centre for Advanced Luminescence Materials
Hong Kong Baptist University
Waterloo Road, Kowloon Tong, Hong Kong (P.R. China)

[c] Q. Wang, Prof. D. Ma, Prof. L. Wang
State Key Laboratory of Polymer Physics and Chemistry
Changchun Institute of Applied Chemistry
Chinese Academy of Sciences
Changchun 130022 (P.R. China)
Fax: (+86) 431-852-628-73
E-mail: mdg1014@ciac.jl.cn

[d] Prof. Z. Lin
Department of Chemistry
The Hong Kong University of Science and Technology
Clearwater Bay, Hong Kong (P.R. China)

Supporting information for this article is available on the WWW under http://dx.doi.org/10.1002/asia.200800226.

ligand charge transfer (^{3}MLCT) and spin-forbidden ligand-based $^3\pi$–π^* states of the phosphors to couple radiatively to the ground state, giving typically high phosphorescent emission efficiencies.

While multicolor emission can be easily achieved for cyclometalated Ir^{III} complexes by adopting different synthetic approaches in the literature,[6] the excited energy state can be modulated by simple variation of the ligand type to endow a phosphorescent complex with specific photophysical and electrochemical traits, color versatility, as well as inhibited aggregation properties. These include changing the degree of conjugation in the structure of the ancillary ligands,[7] and modifying the symmetry and inductive electronic influence of a ligand with different substituents.[8] Electronic effects with inductively electron-donating or -withdrawing groups have also to be considered for their impact on orbital energies.[8c] Many research groups have synthesized and characterized a series of Ir^{III} complexes bearing substituted 2-phenylpyridines as the cyclometalating ligands in which the emissive color of the materials can be finely tuned by synthetic control of the nature and position of the substituents on the aromatic rings.[5c,6a,d,9–11] These research activities inspired us to initiate a systematic study to devise a new strategy in the color tuning of Ir^{III} phosphors by choosing multifunctional ligand chromophores exhibiting different electronic properties. We also pay attention to the effect of isomerism in governing the functional properties of these phosphors and the resulting device performance.[12]

Although iridium phosphors[13] and carbazole derivatives[14] have been widely investigated in the OLED area either as dopants or host materials, a smart combination of both structural moieties is still in its infancy in the OLED field and remains to be studied. Recently, carbazole-based Ir^{III} complexes have been recognized for their prominent role in ensuring high electroluminescence (EL) efficiency by elevating the highest occupied molecular orbital (HOMO) levels and promoting the hole injection/hole transport (HI/HT).[13] To our knowledge, there is no literature precedent or a comprehensive understanding of carbazole derivatives as the building unit in the phosphorescence color tuning of this class of Ir^{III} complexes and work is still limited in studying the Ir–carbazolyl derivatives in the OLED area. Herein, we chose the [3-(*N*-phenylcarbazolyl)]pyridine molecular framework in the synthesis of a series of multifunctional and color-tunable Ir^{III} complexes in which some of them can form pairs of geometrical isomers. The effect of the electronic nature and position of the aryl-ring substituents upon the ground- and excited-state properties was systematically evaluated. Fabrication of electrophosphorescent OLEDs results in remarkable device performance that spans a wide range of emission colors that are suitable for various display technologies and the future realization of promising white-light illumination sources.

Abstract in Chinese:

本文合成了一系列多功能的基于氟及甲基取代的2-[3-(N-苯基咔唑基)]吡啶配体的铱(III)磷光材料。并对其光物理、电化学及电子结构方进行了研究。咔唑基团的富电子性赋予了该类材料良好的空穴注入及传输能力，并且其发光波长可以通过配体及取代基效应从蓝绿色调节到深红色。该类材料表现出优异的电致发光性能，由其制备的磷光发光二极管最大电流效率可达~43.4 cd/A，最大外量子效率可达~12.9 %，最大功率效率可达~33.4 lm/W。因此该研究结果提供了一种新的多功能高效磷光材料设计方法，这对多色 显示技术有重要意义。

Results and Discussion

Preparation and Characterization

A series of [3-(*N*-arylcarbazolyl)]pyridine-based cyclometalating ligands were synthesized and Scheme 1 outlines the synthetic protocol for the ligands **I–IV**. Firstly, the N-arylation of carbazole was achieved by the modified Ullmann condensation between carbazole and the appropriate *p*-iodoarene (X = F, Me) by using CuI/phen/KOH as the catalyst combination[14a] and the product can be prepared on a large scale from the easily accessible carbazole. One equivalent of *N*-bromosuccinimide (NBS) was used to produce the N-arylated 3-bromocarbazole precursors in high yields, which were then converted into their cyclometalating partners **I** and **II** by using a Pd-catalyzed Stille-coupling reaction with 2-(tributylstannyl)pyridine.[13a] The precursors [3-(*N*-phenylcarbazolyl)]pyridines **III** and **IV** were synthesized from palladium-catalyzed cross coupling of 9-phenylcarbazole-3-boronic acid[14] and the commercially available 2-chloro-5-fluoropyridine or 2-chloro-4-methylpyridine, respectively. Indeed, these methods can be readily extended to other similar carbazole derivatives with different substituent groups. Following the ligand syntheses, **I–IV** were easily converted into new homoleptic multifunctional iridium(III) complexes **1–4** (Scheme 2) through a one-step cyclometalation with [Ir(acac)$_3$] (Hacac = acetylacetone) in refluxing glycerol at high temperature (> 200 °C).[15] In this case, the reaction is run with an excess of ligand, which is easily recovered and reused. On the other hand, the iridium-μ-chloro-bridged dimers were synthesized by the reaction of iridium trichloride hydrate with ligands **I–IV** according to a conventional procedure.[9b] The diiridium(III) complexes were then converted to mononuclear iridium(III) complexes **5–8** by replacing the two bridging chlorides with bidentate monoanionic acetylacetonate (acac) ligand. Complexes **1** and **3** (or **2** and **4**; **5** and **7**; **6** and **8**) are isomeric to each other in their respective group. A group of related complexes [Ir(Cz-py)$_3$], [Ir(Cz-py)$_2$(acac)], [Ir(Cz-py-CF$_3$)$_2$(acac)], [Ir(Cz-iq)$_3$], and [Ir(Cz-iq)$_2$(acac)] (Cz = carbazole, py = pyridine, iq = isoquinoline) were also prepared for comparative studies. ^{1}H NMR spectroscopy, mass spectrometry, and elemental analysis of each of the eight complexes is consistent with the expected formulation of their structures. The facial geometry of homoleptic complexes **1–4** is confirmed by the simplicity of the ^{1}H NMR spectral pattern, which indicates that the number of coupled spins is equal to that of the protons on one ligand because the three ligands are magnetically

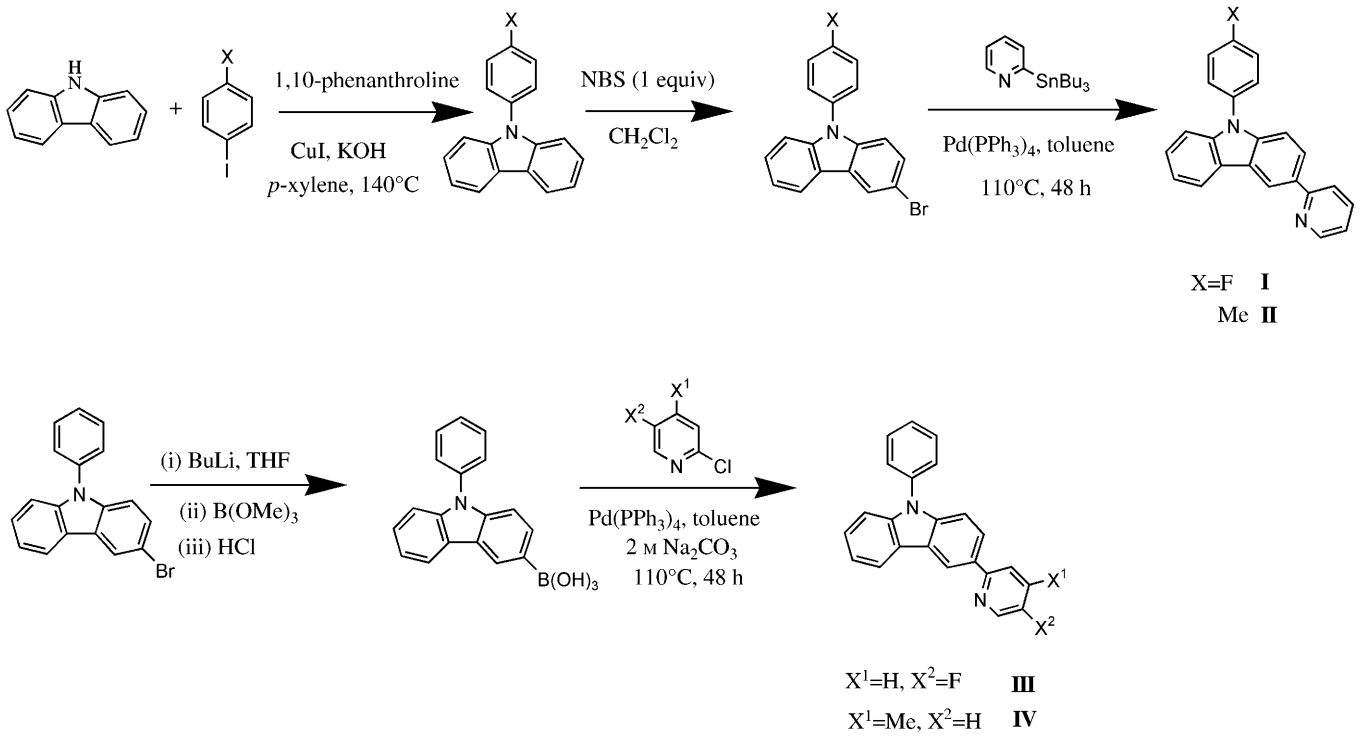

Scheme 1. Synthetic routes to the cyclometalating carbazole-derived ligands **I**-**IV**. NBS = *N*-bromosuccinimide.

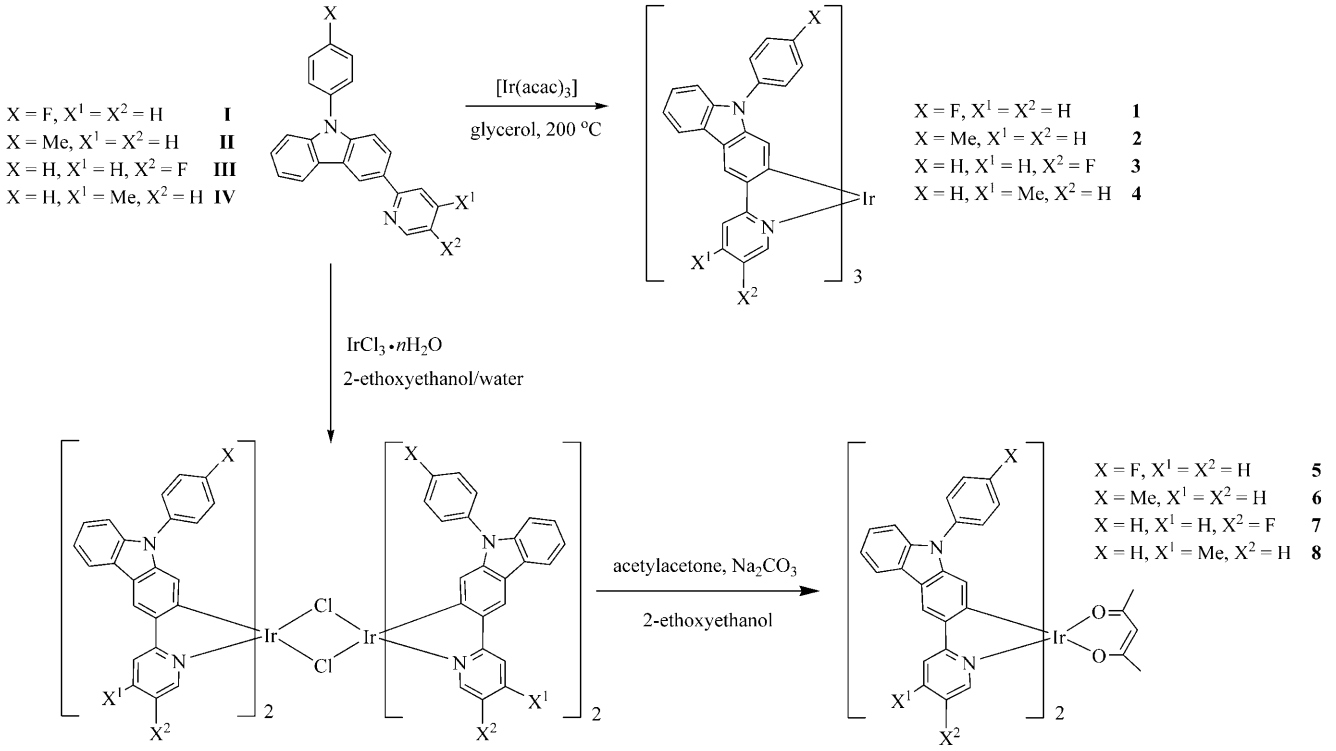

Scheme 2. Synthetic routes to the cyclometalated iridium(III) complexes **1**–**8**.

equivalent owing to the threefold symmetry of the molecule.[16] The molecular structure of **4** was further confirmed by X-ray crystallography (Figure 1).

Crystal Structure Analysis

The ORTEP drawing of **4** is shown in Figure 1. Important bond distances and angles are listed in the Supporting Information, Table S1. The X-ray crystal structure of **4** reveals

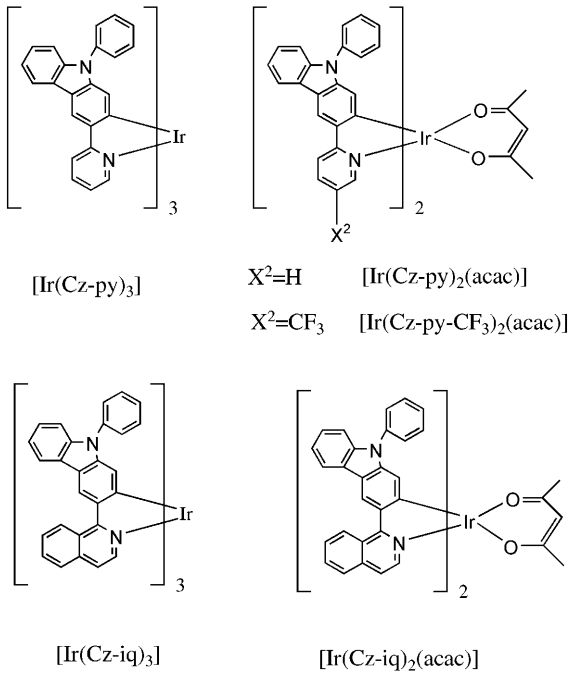

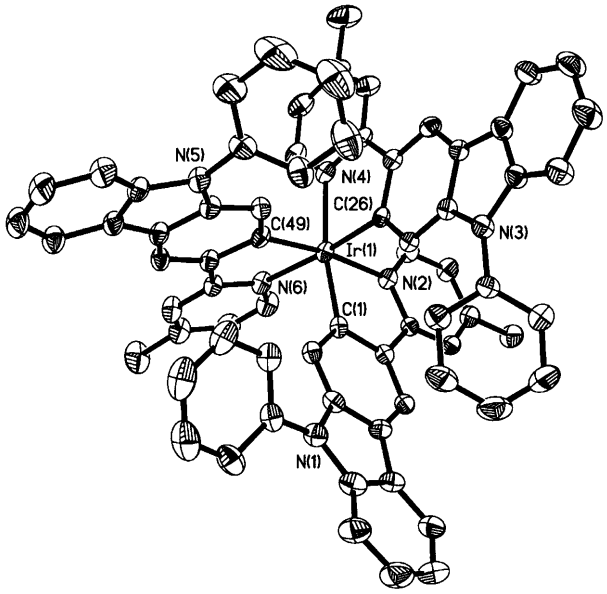

Figure 1. An ORTEP drawing of **4**, with thermal ellipsoids shown at the 25% probability levels. Labels on the carbon atoms (except for those bonded to Ir) and all hydrogen atoms are omitted for clarity.

the central Ir cation to be coordinated by three anionic CN ligands, which reside in a pseudo-octahedral coordination geometry with a facial [Ir(CN)$_3$] arrangement sitting on a threefold axis. Owing to the bulkiness of the cyclometalating ligands, the Ir–C bond lengths are found to be shorter than the Ir–N bond lengths. The Ir–C bond lengths, which range from 1.998(6) to 2.013(5) Å, are close to the values reported for *fac*-[Ir(ppy)$_3$] derivatives (Hppy = 2-phenylpyridine).[10b,17] It should be noted that the sterically crowded ligand results in a deformation with regard to the carbazole and pyridine rings in the complex. The σ-bonded C atoms in the carbazolyl ligand are arranged in a *trans* disposition to the dative-bonded N atoms.

Photophysical and Thermal Properties

The thermal properties of **1**–**8** were investigated through thermogravimetric analysis (TGA) under a nitrogen stream (Table 1). All of the new Ir^{III} phosphor groups are thermally stable up to 340 °C as determined from TGA, which is beneficial for the long-term stability of OLED devices fabricated from these materials. The temperatures that induce a 5% weight reduction are notably different between homoleptic and heteroleptic complexes (420 vs 346 °C for **1** and **5**; 473 vs 377 °C for **2** and **6**; 389 vs 374 °C for **3** and **7**; 479 vs 413 °C for **4** and **8**). These results indicate that the complexes with the acac ligand tend to thermally decompose at relatively lower temperatures but are still sufficiently stable enough for sublimation in vacuum-evaporated OLED fabrication without decomposition. Fluorination of the C–H bonds leads to lower T_{dec} (decomposition temperature) in fluorinated complexes as compared with the unsubstituted complexes (compare 476 °C for [Ir(Cz-py)$_3$]; 404 °C for [Ir(Cz-py)$_2$(acac)]) owing to reduced intermolecular interactions.[18]

The absorption and photoluminescence (PL) spectra (298 K and 77 K) of all the iridium complexes in CH_2Cl_2 solutions are depicted in Figure 2 and the data are summarized in Table 1. The strongest absorption bands in the ultraviolet region are assigned to the spin-allowed intraligand $^1\pi$–π^* transitions. The next lower energy in the shoulder region of $^1\pi$–π^* transitions and the weak broad shoulders extending into the visible region with appreciable intensity are believed to be associated with an admixture of the typical spin-allowed metal-to-ligand charge transfer (^{1}MLCT), spin-orbit coupling enhanced $^3\pi$–π^*, and spin-forbidden ^{3}MLCT transitions. These assignments are made by analogy with previously reported Ir^{III} complexes[6b,19] and the calculations of Hay[20] as well as our computational study (see below). The weakest MLCT absorptions are red-shifted from homoleptic to the corresponding heteroleptic complexes owing to the strong ligand field of the acac ligand. By changing only the X unit on the 9-phenyl ring of the carbazole chromophore from F to Me, there is no apparent difference in the features of the absorption spectra. This suggests that the electronic nature of the lowest excited state is very similar between **1** and **2** (or **5** and **6**; Figure 3). However, when compared with their isomeric complexes, different absorption profiles are observed. The 5-fluoro-substituted pyridyl ligands in **3** and **7** can stabilize the triplet excited states, thereby red-shifting their absorption bands with respect to their isomers **1** and **5**. On the other hand, the 4-methyl substituent on the pyridyl ring tends to destabilize the phosphorescent states, which contributes to a blue-shift in the absorption bands for **4** and **8** relative to their isomeric counterparts **2** and **6**. The present approach appears to be different

Table 1. Photophysical and thermal data for **1**-**8**.

	Absorption (293 K) λ_{abs} [nm][a] CH_2Cl_2	Emission (293 K) λ_{em} [nm] CH_2Cl_2[b]	Φ_P [c]	τ_P [μs] [d]	k_r [s^{-1}]	k_{nr} [s^{-1}]	Emission (77 K) λ_{em} [nm] CH_2Cl_2	τ_P [μs] [d]	T_{dec} [°C]
1	281 (5.45) 315 (7.65) 400 sh (0.16)	513 (2.42)	0.43	0.18	2.3×10^6	3.2×10^6	505	33.9	420
2	286 (3.25) 318 (4.10) 399 sh (0.85)	514 (2.42)	0.43	0.21	2.0×10^6	2.7×10^6	501 525 sh	12.2	473
3	288 (7.00) 312 (7.34) 402 sh (0.63)	528 (2.35)	0.30	0.16	1.9×10^6	4.4×10^6	527	5.1	389
4	293 (2.08) 315 (2.69) 396 sh (0.54)	506 (2.46)	0.47	0.18	2.6×10^6	2.9×10^6	497 528 sh	5.9	479
5	300 (4.79) 325 (4.81) 356 (3.60) 434 sh (0.26)	514 (2.42)	0.45	0.16	2.8×10^6	3.4×10^6	498 530 sh	33.0	346
6	302 (2.02) 323 (2.20) 434 sh (0.44)	515 (2.41)	0.41	0.27	1.5×10^6	2.2×10^6	510	10.4	377
7	308 (5.34) 356 (2.59) 398 (1.66) 440 sh (0.28)	531 (2.34)	0.35	0.22	1.6×10^6	3.0×10^6	521	12.8	374
8	297 (7.72) 325 (9.19) 359 (5.41) 424 sh (0.57)	506 (2.46)	0.41	0.20	2.1×10^6	3.0×10^6	495 530 sh	6.3	413

[a] ε values ($10^4\,M^{-1}cm^{-1}$) are shown in parentheses. [b] Triplet T_1 levels in eV are shown in parentheses. [c] Measured in degassed CH_2Cl_2 relative to *fac*-[Ir(ppy)$_3$] ($\Phi_P = 0.40$), $\lambda_{ex} = 400$ nm. [d] Measured in degassed CH_2Cl_2. sh = shoulder.

from the strategy of inducing the color tuning by carbon-to-nitrogen atom substitution at the cyclometalating ligand framework described recently by Chi and co-workers on iridium(III) complexes with orthometalated quinoxaline ligands.[8d]

Highly intense phosphorescence from the lowest-energy ^{3}MLCT transition was observed for all the iridium(III) complexes **1**–**8** in CH_2Cl_2. Different color was emitted upon photoexcitation depending on the nature and position of the substituents (X, X^1, or X^2) on the cyclometalating ligand. For complexes **1** and **2** and **5** and **6**, they are all strongly luminescent with a bright-green color and their triplet energy levels (T_1 ~2.42 eV) are close to each other and that of *fac*-[Ir(ppy)$_3$] (2.43 eV).[4c] In other words, varying the substituents on the phenyl ring of 9-phenylcarbazole, no matter if they are fluoro or methyl groups, does not show much influence on the spectral feature in terms of peak emission wavelength and the associated vibronic fine structures. These results indicate that the 9-phenyl ring substituent on the carbazole unit plays a minor role in the energy of the lower-lying transitions, which may plausibly be caused by blocking of electron conjugation from the carbazolyl nitrogen atom. For their corresponding geometrical isomers (**3** and **4** and **7** and **8**), we note, however, that a greater substituent effect on the emission position is achieved by attaching an F or Me group to the pyridine ring. Although the pyridine ring mostly contributes to the lowest unoccupied molecular orbital (LUMO) level, the electron-withdrawing fluoro group tends to lower the LUMO energy and thereby decreases the energy gap of the emitting excited state (compare **1** vs **3**, $\Delta\lambda = 15$ nm; **5** vs **7**, $\Delta\lambda = 17$ nm). The electron-donating 4-Me-substituted complexes **4** and **8** (Me group located *para* to the N atom coordinated to the metal center) show the highest energy gap, resulting in a slight spectral blue-shift from **2** and **6**, respectively (compare $\Delta\lambda = 9$ nm for both **2** vs **4** and **6** vs **8**). This can be attributed to the notion that an electron-donating group on pyridine would increase the LUMO energy and the HOMO–LUMO gap.[21] The steric effect of the Me group also forces the carbazole–pyridine aromatic rings out of coplanarity and twists the ligand, which results in reduced delocalization and π-acceptor ability of the molecule. This makes the charge-transfer event more difficult, and a blue spectral shift was observed. Therefore, the phosphorescence wavelength maxima follow the order of **4** < **1** ≈ **2** ≈ [Ir(Cz-py)$_3$] (515 nm)[13a] < **3** < [Ir(Cz-iq)$_3$] (620 nm)[13c] and **8** < **5** ≈ **6** ≈ [Ir(Cz-py)$_2$(acac)] (515 nm)[13e] < **7** < [Ir(Cz-py-CF_3)$_2$(acac)] (555 nm)[13e] < [Ir(Cz-iq)$_2$(acac)] (628 nm)[13c]. The broad emission structure of the PL spectra of **1**–**8** at room temperature confirms that this kind of complex contains less $^3\pi$–π^* character and is mainly in the well-equilibrated ^{3}MLCT state. This is commonly observed with Ir^{III} complexes that bear smaller cyclometalating ligands.[22] Another significant feature of these highly emitting Ir^{III} complexes is the short lifetime of the triplet excited state in

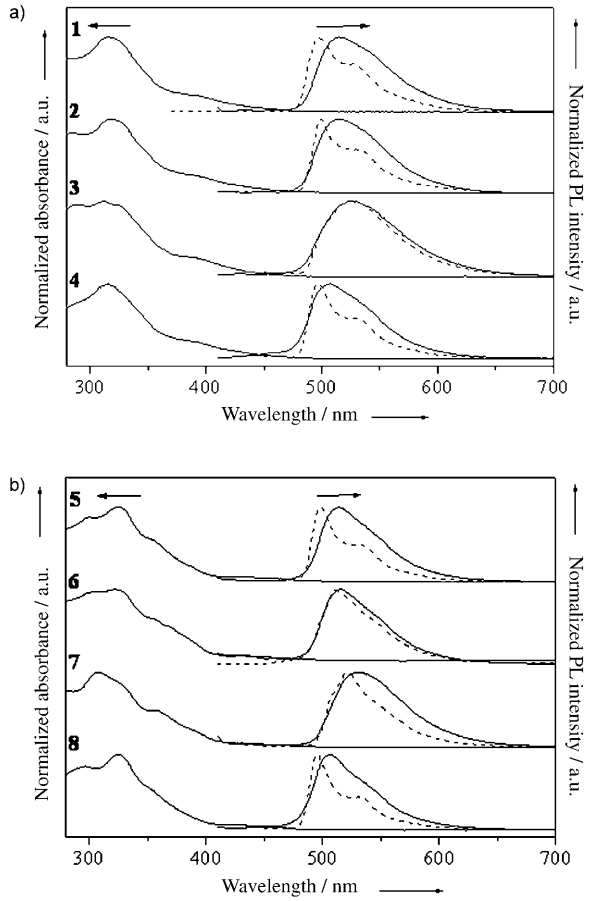

Figure 2. Optical absorption and photoluminescence (PL) spectra of a) **1**–**4** and b) **5**–**8** in CH_2Cl_2 at 293 K (conc. $\sim 10^{-5}$ M). The PL spectra at 77 K are shown as dashed lines.

the sub-microsecond range. These data are indicative of strong spin-orbit coupling, leading to effective intersystem crossing from the singlet to the triplet state.[18,23]

The phosphorescence quantum yields (Φ_P) of the complexes were recorded in degassed solutions at 293 K by using *fac*-[Ir(ppy)$_3$] as the standard ($\Phi_P = 0.40$).[24] Most of the complexes exhibit high solution quantum yields ($\Phi_P =$ 0.30–0.47) at room temperature. Assuming that the emitting state of a complex is formed with unit efficiency, one can calculate the radiative (k_r) and non-radiative (k_{nr}) rate constants by using the relationships $k_r = \Phi_P/\tau_P$ and $k_{nr} = (1-\Phi_P)/\tau_P$.[25] The values are listed in Table 1 and shows that all of the k_r and k_{nr} values have similar orders of magnitude (1.5–2.8×10^6 s^{-1} and 2.2–4.4×10^6 s^{-1}, respectively).

All of the complexes are also intensely luminescent in glassy matrices at 77 K with longer lifetimes than those at ambient temperature. The more structured phosphorescent emission features of the complexes appear at higher energies. In general, most of the complexes show a rigidochromic blue-shift as compared with that recorded at room temperature. The hypsochromic shifts of the peak maximum are caused by solvent reorganization in a fluid solution at room temperature, which stabilizes the charge-transfer states prior to emission. The process is significantly impeded in a rigid matrix at 77 K, and therefore, emission occurs at a higher energy.[7] The structured emission profile also reveals that the mixing between the ^{3}MLCT and $^3\pi$–π^* levels is so effective that the ligand-centered emission predominates upon freezing the matrix. The longer lifetime at 77 K is largely because of the suppression of the thermally nonradiative decay process.

Density Functional Theory (DFT) Calculations

To provide an excellent method for modelling orbital configurations and understanding the nature of excited states of our phosphors, DFT and time-dependent DFT (TDDFT) calculations were carried out by using B3LYP hybrid functional theory (see the Experimental Section). Our TDDFT calculations show that the $S_0 \rightarrow S_1$ transitions correspond to the HOMO→LUMO transitions with non-zero oscillator strengths (Table 2). Therefore, we can place special emphasis on the HOMO–LUMO analyses in the following discussion. The results of DFT calculations show that [Ir(Cz-py)$_3$][13a] and **4** have similar HOMOs and LUMOs in terms of their orbital character (Figure 4). The contour plots show that the HOMOs mainly consist of the "t_{2g}" d orbitals from the metal center that mix with the π orbitals of the phenyl rings that are directly bonded to the metal center. The LUMOs correspond to the lowest π orbital of the conjugated organic ligands, to which the N-containing rings contribute more. In general, electronic effects have been considered owing to their profound influence on orbital energies as well as the relative ease with which electron-withdrawing (e.g., -F, -CF_3) and electron-donating (e.g., -Me) groups can be incorporated into the ligand structure. Electron-withdrawing substituents on pyridine tend to stabilize the HOMO by removing electron density from the metal, whereas the donating moieties have an inverse effect. This relationship is convoluted by the fact that withdrawing groups may also lower the energy of the LUMO (i.e., increasing the electron affinity of the parent ligand). From Figure 4, it is clear that the methyl groups essentially contribute to the LUMO of **4**; the inductive effect is brought about by the electron-donating substituent, which raises the LUMO orbital energy and increases the HOMO–LUMO gap. This is consistent with the DFT results ($E_g = 3.28$ and 3.61 eV for [Ir(Cz-py)$_3$] and **4**, respectively).

Electrochemistry and Electronic Characterization

The electrochemical properties of these Ir^{III} complexes was studied by cyclic voltammetry (CV) by using ferrocene as the internal standard and THF solutions of the complexes containing 0.1 M tetrabutylammonium hexafluorophosphate as the supporting electrolyte at a scan rate of 100 mV s^{-1}. The results are summarized in Table 3. For the redox behavior of the Ir^{III} species, it is generally accepted that the oxidation process involves the iridium moiety of the complexes, and the HOMO levels are mostly owing to the d orbitals of

CHEMISTRY
AN ASIAN JOURNAL

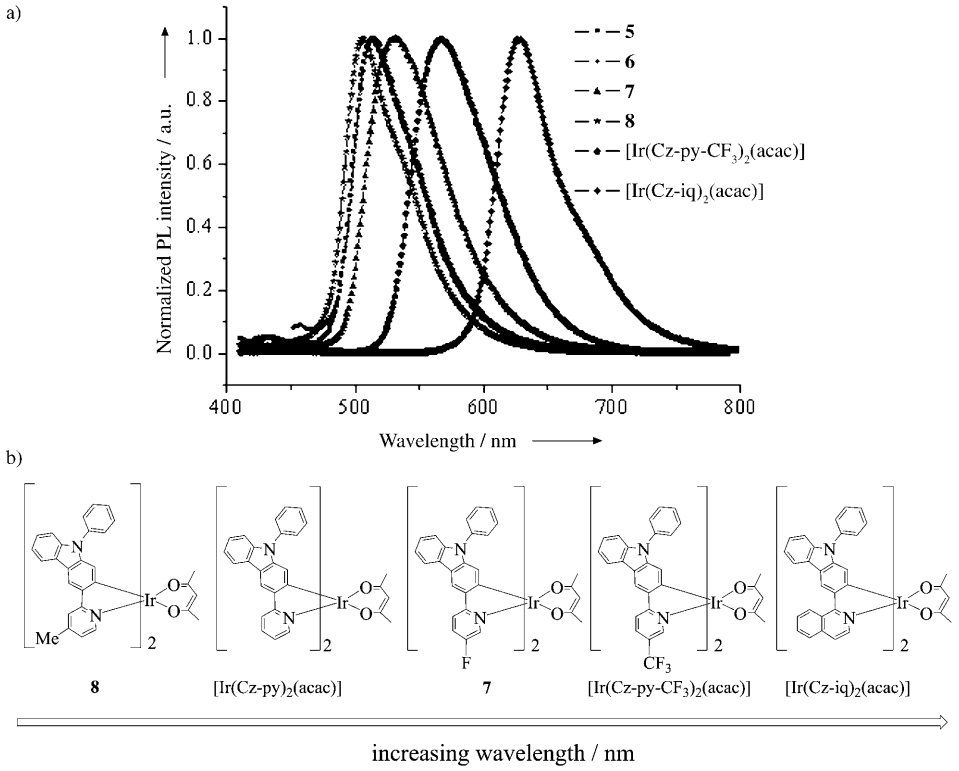

Figure 3. Color tuning of the phosphorescence spectra of various carbazole-based heteroleptic iridium(III) phosphors (**5**–**8**, [Ir(Cz-py-CF_3)$_2$(acac)], and [Ir(Cz-iq)$_2$(acac)]) in CH_2Cl_2 at 293 K.

Table 2. Percentage contribution of the metal d_π orbitals to HOMO and LUMO together with the TDDFT calculation results.

Complex	Contribution of d orbitals to HOMO	Contribution of d orbitals to LUMO	The largest coefficient in the CI expansion of the S_1 state[a]	The oscillator strength (*f*) of the $S_0 \rightarrow S_1$ transition
[Ir(Cz-py)$_3$]	24.5%	3.6%	H→L: 0.53	0.018
4	37.8%	0.9%	H→L: 0.64	0.015

[a] H→L represents the HOMO to LUMO transition. CI stands for configuration interaction.

iridium with some π-orbital contributions from the ligand. The cyclic voltammograms of all the complexes display one-electron reversible oxidation waves assigned to the metal-centered Ir^{III}/Ir^{IV} oxidation couple, which is in accordance with the reported cyclometalated Ir^{III} systems.[26] This electrochemical behavior is consistent with a description of the ligand-localized LUMO states and a HOMO with substantial metal character, as seen in our DFT calculations. These oxidation potentials are lower for the homoleptic complexes than their corresponding heteroleptic complexes, which are in accordance with the fact that the acac ligand with the stronger ligand-field strength could stabilize the HOMO level. From the literature data, the HOMO and LUMO energy levels could be tuned by modification of the substituents on the ppy ring in various *fac*-[Ir(ppy)$_3$] derivatives.[8c] The LUMO level of this kind of complex is mainly attributed to the pyridyl ring of the cyclometalating ligands.[27] As pointed out above, electron-withdrawing substituents tend to stabilize the LUMO level, whereas electron-donating groups show an opposite trend. It is observed that the frontier orbital energy levels are relatively independent of the identity of X on the 9-aryl ring of carbazole. On the contrary, they show a strong dependence on the nature of X^1/X^2 (H, F, or Me) with the stabilizing order of the LUMO level of the pyridyl group substituent being: -Me (**4** and **8**) < -H (**1** or **2** and **5** or **6**) < -F (**3** and **7**; most stabilized) in both homoleptic and heteroleptic series (see Figure S47 in the Supporting Information). Although the moderately electron-donating Me group on pyridine is situated at the *para* position on the pyridine ring in **4** and **8**, which has been shown to be the most sensitive position with respect to both the photophysical and structural aspects, it also has a great influence on the electrochemical properties.[19a] Clearly, the attachment of the electron-withdrawing groups tends to increase the electron affinities of the parent ligands, thereby lowering the LUMO energy levels. As seen in the data in Table 3 for the heteroleptic series, we note the following order for the frontier orbital levels: [Ir(Cz-py)$_2$(acac)] ≈ **5** ≈ **6** ≈ [Ir(Cz-iq)$_2$(acac)] > [Ir(Cz-py-CF_3)$_2$(acac)] (for HOMO) and [Ir(Cz-py)$_2$(acac) ≈ **5** ≈ **6** > [Ir(Cz-py-CF_3)$_2$(acac)] > [Ir(Cz-iq)$_2$(acac)] (for LUMO). Although electron-withdrawing groups located in the *meta* position to the site of coordination in **7** and [Ir(Cz-py-CF_3)$_2$(acac)] increase the field strength of the ligand and concomitantly enhance d-orbital splitting, the notable difference in the observed emission energies between them has been attributed to the mesomeric and inductive effect of the F atom as opposed to the purely inductive ability of the CF_3 group. Therefore, simply changing the electron-donating and electron-withdrawing nature of the pyridyl ligands results in a variation in the electronic properties at the metal center, which in turn will be manifested in the redox propensity and hole/electron-transport features of the resulting complexes. The good reversibility in the electrochemical behavior in each case would be favorable for the overall stability of OLEDs prepared from these Ir phosphors.

As compared with *fac*-[Ir(ppy)$_3$] (−5.05 eV) and [Ir(ppy)$_2$(acac)] (−5.28 eV),[28] the HOMO levels of both series of

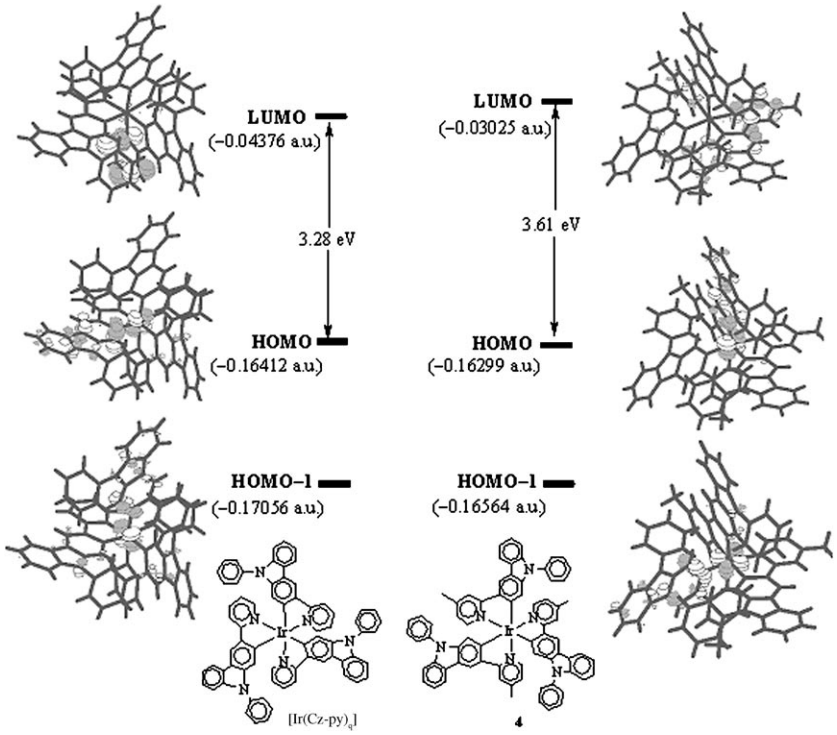

Figure 4. Contour plots of the frontier molecular orbitals for $[Ir(Cz\text{-}py)_3]$ and **4** (1 a.u. = 27.2114 eV).

Table 3. Electrochemical properties and frontier orbital energy levels of **1**-**8**.

Complex	$E_{1/2}^{ox}$ [V][a]	HOMO [eV]	$E_{1/2}^{red}$ [V][a]	LUMO [eV]	E_g [eV]	E_g (DFT) [eV]
1	0.16	−4.96	−2.84	−1.96	3.00	
2	0.13	−4.93	−2.85	−1.95	3.00	
3	0.24	−5.04	−2.72	−2.08	2.96	
4	0.08	−4.88	−2.96	−1.84	3.04	3.61
5	0.23	−5.03	−2.82	−1.98	3.05	
6	0.23	−5.03	−2.82	−1.98	3.05	
7	0.30	−5.10	−2.65	−2.15	2.95	
8	0.21	−5.01	−2.88	−1.92	3.09	
$[Ir(Cz\text{-}py)_3]$	0.15	−4.95	−2.91	−1.89	3.06	3.28 [13a]
$[Ir(Cz\text{-}iq)_3]$	0.16	−4.96	−2.37	−2.43	2.53	2.92 [13c]
$[Ir(Cz\text{-}py)_2(acac)]$	0.23	−5.03	−2.86	−1.94	3.09	3.36 [13e]
$[Ir(Cz\text{-}py\text{-}CF_3)_2(acac)]$	0.40	−5.20	−2.60	−2.20	3.00	3.15 [13e]
$[Ir(Cz\text{-}iq)_2(acac)]$	0.24	−5.04	−2.31	−2.49	2.55	2.84 [13c]

[a] 0.1 M $[Bu_4N]PF_6$ in THF, scan rate 100 mV s^{-1}, versus Fc/Fc^+ couple.

our Ir–carbazolyl homoleptic and heteroleptic complexes are elevated when the electron-rich and electron-donating carbazolyl units are attached to the pyridyl rings, signaling that they have a lower ionization potential than their ppy congeners. This leads to a better HI/HT ability and thus our complexes can serve as dual-functional triplet emitters. Likewise, the HOMO levels of $[Ir(Cz\text{-}iq)_3]$ and $[Ir(Cz\text{-}iq)_2(acac)]$ are shifted to higher-energy levels relative to their 2-phenylisoquinoline congeners, signaling a greater propensity for our carbazole-derived Ir complexes to lose an electron.[13c] This would have a positive contribution in the hole transport and carrier mobility of the thin films in the devices as well as the resulting OLED performance (see below).

Electrophosphorescent OLED Characterization

A good combination of the high phosphorescence quantum efficiencies and thermal stabilities, good film-forming properties, and short triplet-excited-state lifetimes renders this kind of Ir^{III} complex advantageous for efficient optoelectronic devices. Most of the complexes have been utilized for OLED device fabrication by using vacuum-evaporation techniques in varied structures (Figure 5 and Table 4, also see Figure S2 in the Supporting Information). Preliminary studies have been performed on the devices with the following configuration: ITO/NPB (40 nm; ITO = indium tin oxide, NPB = 4,4′-bis[*N*-(1-naphthyl)-*N*-phenyl-amino]biphenyl)/7 % **1** in CBP (20 nm; CBP = 4,4′-*N*,*N*′-dicarbazolebiphenyl)/BCP (8 nm; BCP = 2,9-dimethyl-4,7-diphenyl-1,10-phenanthroline)/Alq_3 (20 nm; Alq_3 = *tris*[8-hydroxyquinoline)/Mg:Ag (200 nm; device **I**).[13a] ITO acts as the anode and NPB as the hole-transporting material. A thin hole and exciton blocking barrier layer of BCP inserted between CBP and the electron-transporting Alq_3 was necessary to confine excitons within the luminescent zone and hence maintain high efficiencies. We chose CBP as the host material for our complexes because of its theoretical confirmation of favorable triplet energy.[3,11a,29] For devices **II**–**IX**, LiF (1 nm) acts as the electron-injection layer and Al as the cathode. For comparison, devices with 4,7-diphenyl-1,10-phenanthroline (BPhen) to replace BCP/Alq_3 as the electron-transporting and electron-injection layer were also prepared with the configuration of ITO/NPB (60 nm)/x % Ir in CBP (30 nm)/BPhen (20 nm)/LiF (1 nm)/Al (60 nm; devices **II**–**VI**). Different dopant concentrations were used to find out the optimum weight percentages for devices with the highest efficiencies.

Each of the devices exhibits a strong voltage-independent electroluminescent (EL) signal with no guest-concentration dependence, which is only slightly blue-shifted from the corresponding photoluminescence spectrum observed in the so-

CHEMISTRY
AN ASIAN JOURNAL

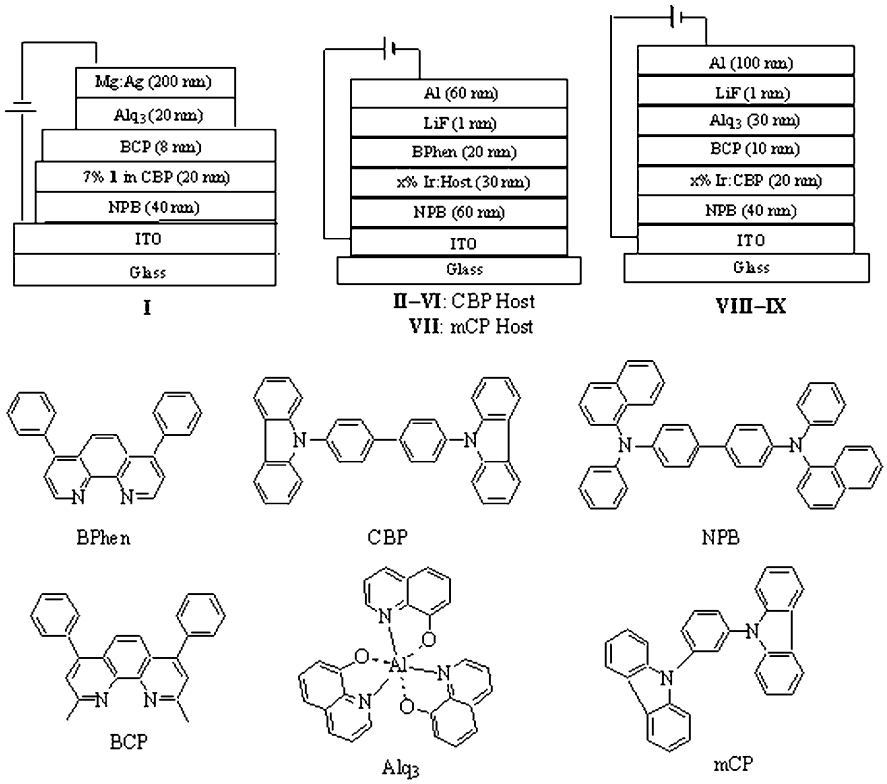

Figure 5. The general structure for OLED devices and the molecular structures of the relevant compounds used in these devices.

lution state. The close resemblance between their PL and EL spectra indicates the absence of aggregation or π stacking at all the doping levels examined, and the origin of EL emission from the triplet excited states was confirmed. In the majority of cases, the EL spectra consist only of the phosphor emission without any residual emission from the host and/or adjacent layers, even at high drive currents, which is an indication of complete energy transfer from the host exciton to the phosphor in the EL process. Figure 6 shows the EL spectra of devices fabricated with selected dopants as well as those for [Ir(Cz-iq)$_3$], [Ir(Cz-py-CF$_3$)$_2$(acac)], and [Ir(Cz-iq)$_2$(acac)]. Most of the devices exhibit remarkable OLED performance with a narrow full width at half maximum (FWHM) in each case. We can surmise that it is probably the carbazolyl structural moiety that brings about a more balanced electron and hole recombination in the host matrix of CBP. This therefore increases the overall device efficiency in many cases. Although all attempts to obtain the homoleptic counterpart of [Ir(Cz-py-CF$_3$)$_2$(acac)] with 5-trifluoromethyl-2-[3-(*N*-phenylcarbazolyl)]pyridine ligand have met with little success so far (presumably owing to the unfavorable steric hindrance in the presence of three bulky CF$_3$ groups in the molecule), it is clear from Figure 6b (for the heteroleptic series) that the EL color change follows the same trend as the PL spectra, which shifts from blue–green, green–yellow, and orange to deep red for different ligand structures. Saliently, it was also recently demonstrated that the orange phosphor [Ir(Cz-py-CF$_3$)$_2$(acac)] can be used to afford high-performance white light OLEDs by combining with some suitable blue dopants.[13b,e] Although the carbazolyl group is critical in improving the EL efficiency and charge transport, versatile color tuning of this class of highly efficient OLEDs was readily achieved by modifying the substituent on the pyridyl ring. Thus, the present work focuses on methods for synthetically tailoring the properties of bis-cyclometalated iridium(III) materials. All of the devices with BPhen as the electron-transporting layer show low turn-on voltages of no more than 3.6 V, which is lower than that of device **I** (4.8 V). This can be attributed to a more balanced electron transport for BPhen[30] as compared with the combined BCP/Alq$_3$ layer in **I**. The decreased device-operation voltage will result in an increased power efficiency owing to the more effective injection and transport of charges.[31] In addition, the LUMO offset (approximately 0.2 eV) between CBP and BPhen is smaller than that for BCP (0.3 eV; LUMO of CPB: −3.2 eV; BPhen: −3.0 eV; BCP: −2.9 eV). Therefore, electron injection from BPhen to CPB is more efficient and recombination of charges occurs predominantly on CPB (given that BPhen and BCP have the same HOMO value of −6.4 eV such that there would be negligible influence on hole transportation). For **4** and **7** (with the PL maximum at 506 and 531 nm, respectively), the Commission Internationale de l'Eclairage (CIE) coordinates are shifted from (0.23,0.61) for device **IV** to (0.31,0.62) for device **V**, with the color shift from bright green to greenish–yellow.

Among all the complexes, the best performance was achieved in the device based on complex **2** at 10 wt.% doping concentration. A maximum brightness of 28400 cd m^{-2} was achieved at a current density of $J=200$ mA cm^{-2}, with the maximum luminance (η_L), quantum (η_{ext}), and power (η_p) efficiencies of 43.42 cd A^{-1}, 12.93%, and 33.36 Lm W^{-1}, respectively. Figure 7 depicts the current–voltage–luminance (*I*–*V*–*L*) characteristics of device **II** at different doping concentrations. The gradual decrease of the OLED efficiency with increasing current density is predominantly attributed to the triplet–triplet annihilation of the phosphor-bound excitons[32] and field-induced quenching effects.[33] No aggregation or self-quenching was observed even at the doping concentration of up to 10 wt.% for the devices. Obviously, re-

Table 4. Key data for the performance of vacuum-evaporated electrophosphorescent OLEDs.

Device	Dopant	$V_{turn-on}$ [V]	Luminance L [cd m^{-2}][a]	η_L [cd A^{-1}][a]	η_{ext} [%][a]	η_p [Lm W^{-1}][a]	λ_{max} [nm][b]	CIE
I	**1** (7%)	4.8	19360 (12)	21.35 (5.6)	6.69 (5.6)	12.33 (5.2)	508 (57)	0.27, 0.60
II	**2** (6%)	3.5	25800 (9.8)	34.73 (4.0)	10.54 (4.0)	27.51 (3.9)	504 (57)	0.23, 0.60
	2 (8%)	3.4	28240 (8.9)	39.55 (3.9)	11.88 (3.9)	33.16 (3.6)	508 (58)	0.24, 0.61
	2 (10%)	3.6	28400 (9.2)	43.42 (4.2)	12.93 (4.0)	33.36 (4.0)	508 (54)	0.25, 0.62
III	**3** (6%)	3.6	22080 (9.8)	12.91 (4.8)	4.09 (4.8)	8.46 (4.8)	512 (63)	0.25, 0.57
	3 (8%)	3.5	31160 (9.8)	23.36 (4.0)	6.85 (4.0)	18.71 (3.8)	512 (60)	0.26, 0.57
	3 (10%)	3.4	21270 (9.1)	21.94 (4.0)	6.70 (4.0)	17.63 (3.9)	512 (65)	0.27, 0.62
IV	**4** (6%)	3.5	22710 (8.4)	35.62 (4.0)	11.50 (4.0)	28.23 (3.7)	500 (55)	0.22, 0.58
	4 (8%)	3.5	22800 (8.2)	33.26 (4.9)	10.36 (4.9)	22.32 (4.3)	504 (59)	0.23, 0.61
	4 (11%)	3.5	20650 (7.3)	24.70 (5.0)	7.80 (5.0)	19.92 (3.8)	504 (56)	0.23, 0.61
V	**7** (6%)	3.7	23190 (9.7)	20.13 (4.6)	5.71 (4.6)	14.34 (4.3)	524 (65)	0.30, 0.58
	7 (8%)	3.5	26730 (9.4)	37.70 (4.8)	10.23 (4.8)	26.15 (4.2)	524 (64)	0.31, 0.62
	7 (10%)	3.5	24560 (8.7)	23.48 (4.0)	6.38 (4.0)	19.40 (3.7)	528 (64)	0.31, 0.61
VI	**8** (4%)	3.5	23880 (9.4)	23.98 (4.0)	7.31 (4.0)	18.76 (3.8)	508 (54)	0.23, 0.61
	8 (6%)	3.3	22100 (8.7)	36.00 (3.8)	10.77 (3.8)	30.67 (3.6)	508 (54)	0.23, 0.63
	8 (8%)	3.3	22100 (8.7)	29.36 (3.8)	8.76 (3.8)	25.45 (3.5)	508 (57)	0.24, 0.63
VII	**2** (6%)	3.9	18230 (9.9)	17.97 (4.1)	5.99 (4.1)	13.94 (4.1)	506 (60)	0.21, 0.43
VIII	**3** (4%)	5.8	33955 (16.1)	15.64 (10.9)	4.99 (11.7)	4.65 (10.5)	530 (90)	0.36, 0.59
	3 (6%)	6.2	35791 (15.9)	18.38 (11.5)	5.33 (11.5)	5.23 (10.9)	530 (90)	0.36, 0.59
	3 (8%)	6.0	38836 (16.5)	17.31 (11.7)	5.54 (12.3)	4.92 (10.9)	530 (90)	0.36, 0.59
	3 (10%)	6.5	30719 (16.7)	13.81 (11.5)	4.01 (11.5)	3.81 (10.9)	530 (90)	0.36, 0.59
IX	**7** (4%)	4.0	48270 (15.3)	24.41 (9.3)	6.68 (9.3)	8.24 (9.3)	533 (76)	0.37, 0.59
	7 (6%)	3.7	48438 (15.3)	32.36 (9.1)	8.85 (9.1)	11.17 (9.1)	533 (76)	0.37, 0.59
	7 (8%)	3.6	48340 (14.1)	37.96 (9.5)	10.38 (9.5)	13.14 (8.7)	533 (76)	0.37, 0.59
	7 (10%)	3.6	47570 (13.9)	37.41 (8.7)	10.23 (8.7)	13.50 (8.7)	533 (76)	0.37, 0.59
	[Ir(Cz-py)$_3$] (4%) [13a]	4.4	14730 (12)	38.01 (5.2)	11.56 (5.2)	23.92 (4.8)	508 (57)	0.24, 0.63
	[Ir(Cz-py)$_2$(acac)] (6%) [13e]	3.6	24730 (10.0)	21.56 (4.4)	6.15 (4.4)	16.39 (4.1)	512 (58)	0.25, 0.63
	[Ir(Cz-py-CF$_3$)$_2$(acac)] (4%) [13e]	3.6	48587 (11.7)	12.36 (5.5)	40.22 (5.5)	23.95 (4.9)	556 (70)	0.44, 0.51
	[Ir(Cz-iq)$_3$] (4%) [13c]	4.6	5846 (24.7)	11.00 (5.5)	10.87 (5.5)	6.16 (5.3)	624 (65)	0.66, 0.34
	[Ir(Cz-iq)$_2$(acac)] (4%) [13c]	4.2	10750 (19.5)	10.15 (6.3)	11.76 (6.3)	5.25 (5.1)	628 (60)	0.68, 0.33

[a] Maximum values of the devices. Values in parentheses are the voltages at which they were obtained; [b] Full width at half maximum (FWHM) in nm shown in parentheses.

placement of the CPB layer by 1,3-bis(9-carbazolyl)benzene (mCP) as the host material resulted in lower efficiencies. So, the EL performance of device **VII** is much poorer than those of **II** at each dopant level. This may arise from the higher LUMO level of mCP (−2.3 eV) than CBP (LUMO: −3.0 eV), which lead to insufficient electron blocking at the interface of NPB/mCP. A minor emission from NPB (at ~450 nm)[30] was found in device **VII** when a mCP host was employed (see the Supporting Information). The lower triplet energy of CBP (λ_{max} ~460 nm)[35] compared with that of mCP (λ_{max} ~410 nm)[36] ensures a more efficient energy transfer for the triplet of CBP to the triplet states of the Ir dopant.

As compared with its isomer (**4** in device **IV**), the best performance was achieved at 6 wt.% of **4** with the expected blue-shift in the EL peak, but the efficiencies are still respectable with a maximum brightness of 22710 cd m^{-2} at 8.4 V, η_L of 35.62 cd A^{-1}, η_{ext} of 11.50%, and η_p of 28.23 Lm W^{-1} at ~4.0 V, which are slightly higher than those for device **II** at the same doping concentration (Figure 8). However, the efficiencies are depressed as the doping concentration increases. The performance of its heteroleptic congener is also impressive (device **VI**). The best EL efficiencies were observed at 6 wt.% with a maximum η_{ext} of 10.77%, η_L of 36.00 cd A^{-1}, and η_p of 30.67 Lm W^{-1}.

Fluorinated pyridyl-substituted complexes **3** (device **III**) and its heteroleptic analogue **7** (device **V**) also show satisfactory EL results. The luminance of device **V** was 26730 cd m^{-2} at 9.4 V for the 8 wt.% level. This resulted in the maximum η_{ext} of 10.23%, η_L of 37.70 cd A^{-1}, and η_p of 26.15 Lm W^{-1}. A poorer performance with the homoleptic counterpart (device **III**) was noted. Moreover, these two complexes (**3** and **7**) can be used to fabricate efficient OLEDs with another configuration: ITO/NPB (40 nm)/CBP:**3** or **7** (20 nm)/BCP (10 nm)/Alq_3 (30 nm)/LiF/Al. Our results show that optimum device performance is achieved at the doping level of 8 wt.% of **7** (device **IX**) with a maximum luminance of 48340 cd m^{-2} at 14 V, η_L of 37.96 cd A^{-1} at 9.5 V, η_{ext} of 10.38% at 9.5 V, and η_p of 13.14 Lm W^{-1} at 8.7 V. A lower power efficiency was observed as compared with device **V** when BCP/Alq_3 was used as the electron-transporting layer for the same reason as mentioned previously. A similar observation was also found with the complex **3** (device **III** vs **VIII**). Additionally, the effect of substitution in the ligand structure would have a clear impact on the device performance. For instance, the HOMO levels for **3** and **7** (−5.04 and −5.10 eV, respectively) are elevated to a lesser extent than the other three phosphors in each series relative to [Ir(ppy)$_3$] and [Ir(ppy)$_2$(acac)], resulting in their lower EL efficiencies among **1**–**4** and **5**–**8**.

CHEMISTRY
AN ASIAN JOURNAL

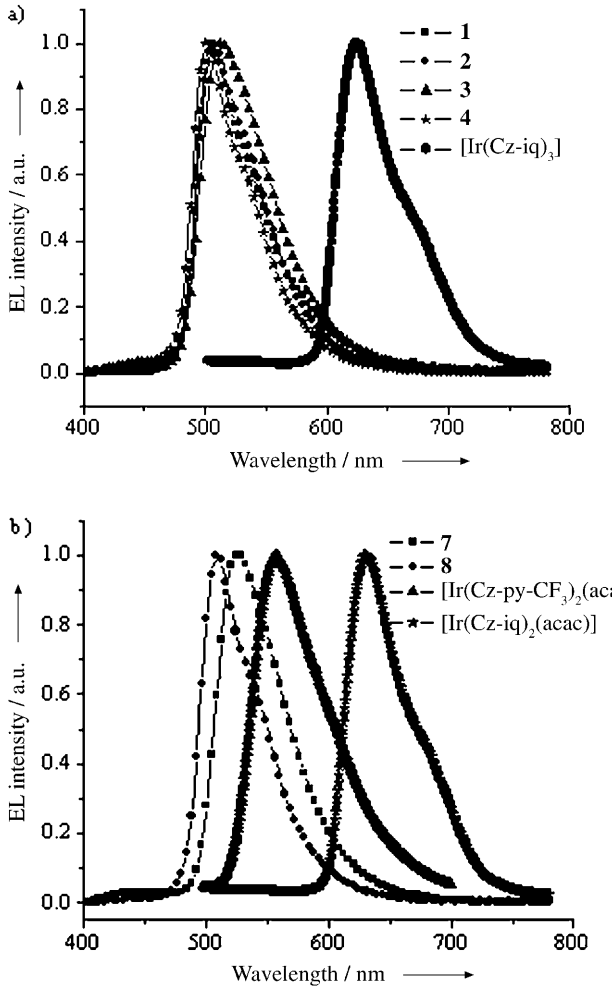

Figure 6. EL spectra of a) **1**–**4** and [Ir(Cz-iq)$_3$] and b) **7**-**8**, [Ir(Cz-py-CF$_3$)$_2$(acac)] and [Ir(Cz-iq)$_2$(acac)].

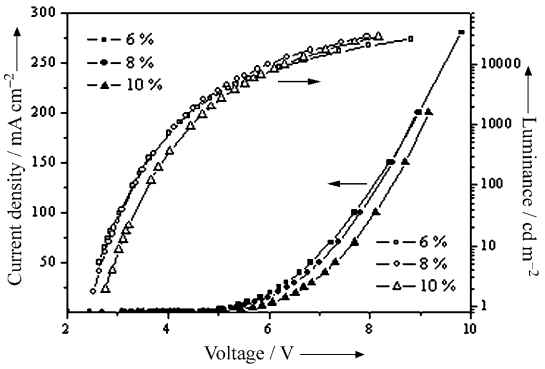

Figure 7. *I*–*V*–*L* characteristics of the electrophosphorescent OLED devices **II** at different doping levels.

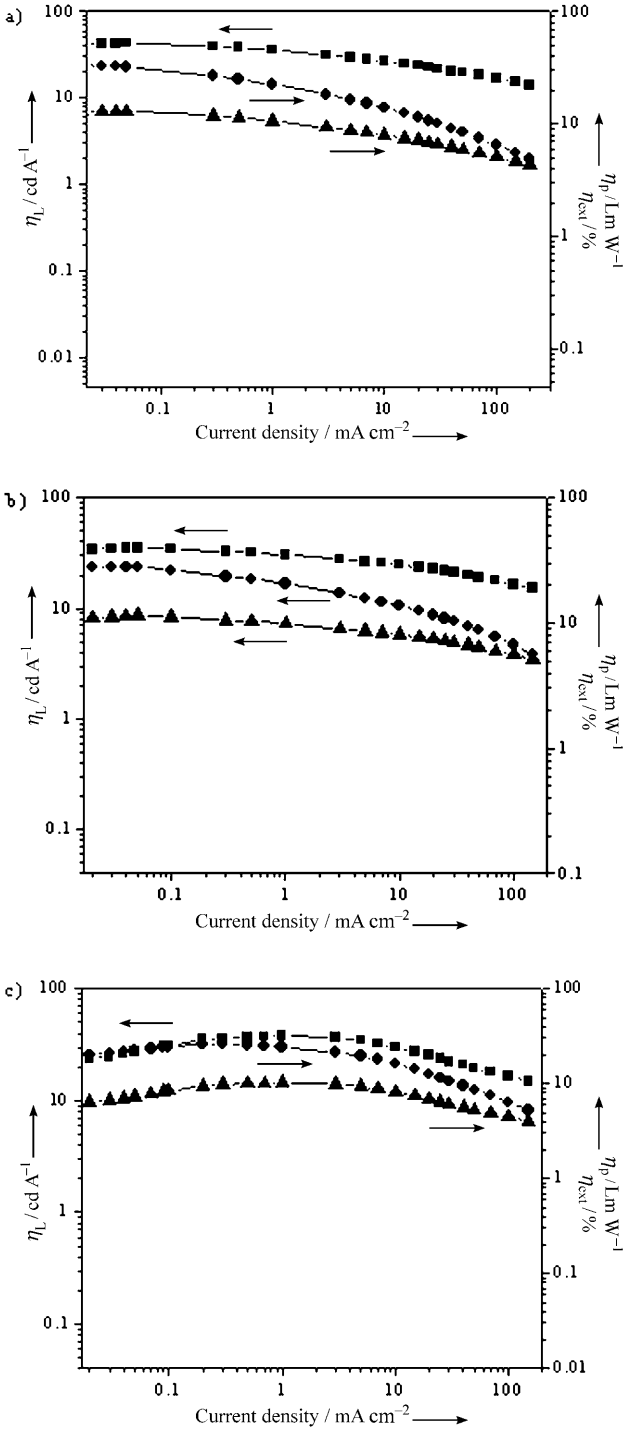

Figure 8. Luminance (■), power (●), and external quantum (▲) efficiencies as a function of current density for OLED devices a) **II** at 10 wt.%, b) **IV** at 6 wt.% and c) **V** at 8 wt.%.

Conclusions

Herein, we focus on the interesting work in the design and utility of multicomponent iridium(III)–carbazolyl metallophosphors with improved charge-transporting properties for high-performance color-switchable OLEDs. We have shown that luminescent iridium(III) compounds can be incorporated into multifunctional conjugated organic architectures, which offer a very versatile avenue for emission-color tuning of iridophosphors through the facile derivatization of the carbazolylpyridyl moiety. The short triplet-excited-state lifetime together with the high phosphorescence yield would

favor the realization of highly efficient devices. These molecules are capable of performing separate functional roles (i.e., hole transport as well as triplet emission) in a single molecule, and the resulting OLED devices show superior performance to that of a state-of-the-art phosphor with the neat 2-phenylpyridine group. We have extensively investigated the effect of the position of aryl/heteroaryl ring substituents on the photophysics, electrochemistry, and electrophosphorescent properties of the materials. The performance of these materials in photophysical applications depends heavily on the ligand substituent effects and their excited-state properties. It is possible to control the energy of the lowest triplet excited state by deliberately adjusting the energy of metal and ligand orbitals, which can be achieved through substituent effects or by changing the ligand parent structure entirely (e.g., Cz-py vs Cz-iq). Although the redox and luminescence properties of these metalated phosphors are rather insensitive to the position of the aryl-ring substituent on carbazole, there is a strong dependency between the emission energy and the electronic properties of the pyridyl-ring substituent. Given the ease of synthesis and color tunability as well as performance advantages, the present demonstration of Ir–carbazole derivatives as highly efficient electrophosphors blows fresh air into the OLED field and may lead to the ultimate goal to realize a full-color spectrum for flat-panel displays and practical white-light illumination sources.

Experimental Section

General

All reactions were performed under nitrogen. Solvents were carefully dried and distilled from appropriate drying agents prior to use. Commercially available reagents were used without further purification unless otherwise stated. 9-Arylcarbazoles (X = F, Me),[37] $[Ir(Cz\text{-}py)_3]$,[13a] $[Ir(Cz\text{-}py)_2(acac)]$,[13e] $[Ir(Cz\text{-}py\text{-}CF_3)_2(acac)]$,[13e] $[Ir(Cz\text{-}iq)_3]$,[13c] and $[Ir(Cz\text{-}iq)_2(acac)]$[13c] were prepared according to the published methods. All reactions were monitored by TLC with Merck pre-coated glass plates. Flash column chromatography and preparative TLC were carried out by using silica gel from Merck (230–400 mesh). Fast atom bombardment (FAB) mass spectra were recorded on a Finnigan MAT SSQ710 system. NMR spectra were measured in deuterated solvent on a Varian Inova 400 MHz FT-NMR spectrometer; chemical shifts were quoted relative to the internal standard tetramethylsilane for ^1H and $^{13}C\{^1H\}$ NMR data.

Physical Measurements

Optical absorption spectra were obtained on a HP-8453 spectrophotometer. The photoluminescent properties and lifetimes of the compounds were probed on the Photon Technology International (PTI) Fluorescence Master Series QM1 system. The phosphorescence quantum yields were determined in CH_2Cl_2 solutions at 293 K against *fac*-$[Ir(ppy)_3]$ as a reference ($\Phi_P = 0.40$).[24] For phosphorescence lifetime measurements, samples were prepared in CH_2Cl_2 solutions and were degassed using at least three freeze–pump–thaw cycles on a grease-free, turbo-pumped, high-vacuum line to a pressure of approximately 5×10^{-5} Torr in each cycle. Phosphorescence lifetimes were measured in degassed toluene with a Lecroy Wave Runner 6100 digital oscilloscope by using the third harmonic of a Nd:YAG laser ($\lambda = 355$ nm, pulse width = 8 ns) as the excitation source (Spectra-Physics Quantum-Ray). The decay curves were analyzed by using a Marquardt-based nonlinear least-squares fitting routine and were shown to follow a single-exponential function in each case according to $I = I_0 + A\exp(-t/\tau)$. The associated error with measured lifetimes is ±5%. A conventional three-electrode configuration consisting of a glassy carbon working electrode and Pt-wire counter and reference electrodes was used. The solvent in all measurements was THF and the supporting electrolyte was 0.1 M $[Bu_4N]PF_6$. Ferrocene was added as an internal standard after each set of measurements, and all potentials reported were quoted with reference to the ferrocene–ferrocenium (Fc/Fc^+) couple at a scan rate of 100 mV s^{-1}. The oxidation ($E_{1/2}^{ox}$) and reduction ($E_{1/2}^{red}$) potentials were used to determine the HOMO and LUMO energy levels by using the equations $E_{HOMO} = -(E_{1/2}^{ox} + 4.8)$ eV and $E_{LUMO} = -(E_{1/2}^{red} + 4.8)$ eV, which were calculated by using the internal standard ferrocene value of −4.8 eV with respect to the vacuum level. Thermal analyses were performed with Perkin–Elmer TGA6 thermal analyzers. DFT calculations at the B3LYP level were performed based on experimental geometries from the X-ray diffraction data. The basis set used for C, N, O, and H atoms was 6–31G, whereas effective core potentials with a LanL2DZ basis set were employed for Ir atom.[38] All the calculations were carried out by using the Gaussian 03 program. Molecular orbitals obtained from the B3LYP calculations were plotted by using the Molden 3.7 program written by Schaftenaar.[39]

General Procedures of Synthesis of Homoleptic Iridium(III) Complexes ***1–4***

All of the homoleptic iridium(III) complexes were synthesized by the same synthetic routes by heating a solution of $[Ir(acac)_3]$ and 3.5 molar equivalents of the corresponding ligand in glycerol (15 mL) and the mixture was heated to 200 °C under a N_2 atmosphere. After 18 h, the reaction mixture was then cooled down to room temperature and water was added. The resulting mixture was extracted with CH_2Cl_2 and the organic layer was dried over $MgSO_4$. Upon solvent removal under vacuum, a pure sample of each complex was obtained by column chromatography eluting with a CH_2Cl_2/hexane mixture.

1: A pale-yellow solid was obtained in 53% yield. MS (FAB): *m/z* 1204 [M^+]. ^1H NMR ($CDCl_3$): $\delta = 8.34$ (s, 3H, Ar), 8.04–8.02 (d, 6H, J = 6.8 Hz, Ar), 7.66–7.61 (m, 6H, Ar), 7.28–7.22 (m, 9H, Ar), 6.87–6.82 (m, 9H, Ar), 6.70 (s, 3H, Ar), 6.30 (t, 6H, $J = 8.9$ Hz, Ar) ppm. Anal. calcd. for $C_{69}H_{42}N_6F_3Ir$: C 68.81, H 3.52, N 6.98; found: C 68.65, H 3.44, N 6.64.

2: A pale-yellow solid was obtained in 20% yield. MS (FAB): *m/z* 1192 [M^+]. ^1H NMR ([D_6]DMSO): $\delta = 8.54$ (s, 3H, Ar), 8.30–8.23 (m, 3H, Ar), 8.11 (d, 3H, $J = 8.1$ Hz, Ar), 7.82–7.80 (m, 6H, Ar), 7.37–7.13 (m, 18H, Ar), 6.97 (d, 4H, $J = 8.1$ Hz, Ar), 6.59 (s, 1H, Ar), 6.45 (d, 4H, J = 8.1 Hz, Ar), 1.42 ppm (s, 9H, CH_3). Anal. calcd. for $C_{72}H_{51}N_6Ir$: C 72.52, H 4.31, N 7.05; found: C 72.33, H 4.40, N 7.24.

3: A pale-yellow solid was obtained in 30% yield. MS (FAB): *m/z* 1204 [M^+]. ^1H NMR ($CDCl_3$): $\delta = 8.21$ (s, 3H, Ar), 8.02--7.97 (m, 6H, Ar), 7.62 (m, 3H, Ar), 7.44–7.40 (m, 3H, Ar), 7.32–7.30 (m, 6H, Ar), 7.21–7.19 (m, 3H, Ar), 6.87 (d, 6H, $J = 5.4$ Hz, Ar), 6.60 (t, 6H, $J = 10.8$ Hz, Ar), 6.46 (s, 3H, Ar), 6.36 ppm (d, 3H, $J = 8.1$ Hz, Ar). Anal. calcd. for $C_{69}H_{42}N_6F_3Ir$: C 68.81, H 3.52, N 6.98; found: C 68.63, H 3.44, N 6.64.

4: A pale-yellow solid was obtained in 20% yield. MS (FAB): *m/z* 1192 [M^+]. ^1H NMR ([D_6]acetone): $\delta = 8.51$ (s, 3H, Ar), 8.09 (d, 3H, J = 5.4 Hz, Ar), 8.04 (s, 3H, Ar), 7.72 (d, 3H, $J = 2.7$ Hz, Ar), 7.35--7.29 (m, 6H, Ar), 7.21–7.17 (m, 3H, Ar), 7.05–7.03 (m, 6H, Ar), 6.89–6.88 (m, 3H, Ar), 6.81 (s, 3H, Ar), 6.72 (t, 6H, $J = 10.8$ Hz, Ar), 6.48 (t, 3H, J = 10.8 Hz, Ar), 2.44 ppm (s, 9H, Me). Anal. calcd. for $C_{72}H_{51}N_6Ir$: C 72.52, H 4.31, N 7.05; found: C 72.34, H 4.45, N 6.84.

General Procedures of Synthesis of Heteroleptic Iridium(III) Complexes ***5–8***

The heteroleptic iridium(III) complexes were synthesized by reacting $IrCl_3 \cdot 3H_2O$ with 3 equivalents of the corresponding cyclometalating ligand in a mixture of 2-ethoxyethanol and water (6:2, v/v). The mixture was refluxed for 24 h and then cooled to room temperature. A precipitate gradually formed during the reaction. The precipitate was collected by filtration and washed with ethanol followed by hexane. The solid was then dried under vacuum to give the crude Ir^{III} dimer for subsequent reaction. Without further purification, this crude dimer was mixed with 10 equivalents of Na_2CO_3 in 2-ethoxyethanol. Acetylacetone (3 equiva-

lents) were added and the reaction mixture was then refluxed for 16 h. After the mixture was cooled to room temperature, water was added and extracted with CH_2Cl_2. The organic layer was collected and the solvent was subsequently removed. The residue was then purified by using preparative TLC plates eluting with CH_2Cl_2/hexane.

5: A pale-yellow powder was obtained in 19% yield. MS (FAB): *m/z* 966 [M^+].^{1}H NMR ($CDCl_3$): $\delta = 8.46$ (d, 2H, $J = 8.1$ Hz, Ar), 8.25 (s, 2H, Ar), 7.96 (d, 4H, $J = 8.1$ Hz, Ar), 7.68 (t, 2H, $J = 8.1$ Hz, Ar), 7.25--7.02 (m, 16H, Ar), 6.12 (s, 2H, Ar), 5.23 (s, 1H, acac), 1.79 ppm (s, 6H, CH_3). ^{13}C NMR ($CDCl_3$): $\delta = 184.44$ (CO), 168.65, 147.93, 146.05, 142.25, 139.80, 137.48, 136.36, 133.58, 128.32, 128.20, 124.63, 124.24, 120.19, 119.84, 118.72, 117.92, 117.67, 115.95, 115.62, 112.00, 109.23 (Ar), 100.53 (CH), 28.91 ppm (CH_3). Anal. calcd. for $C_{51}H_{35}N_4F_2O_2Ir$: C 63.41, H 3.65, N 5.80; found: C 63.22, H 3.70, N 5.89.

6: A pale-yellow powder was obtained in 23% yield. MS (FAB): *m/z* 958 [M^+].^{1}H NMR ($CDCl_3$): $\delta = 8.46$ (d, 2H, $J = 6.4$ Hz, Ar), 8.26 (s, 2H, Ar), 7.96 (d, 4H, Ar), 7.68–7.64 (d, 2H, $J = 8.6$ Hz, Ar), 7.21–7.19 (m, 4H, Ar), 7.17 (s, 8H, Ar), 7.13–7.09 (m, 2H, Ar), 7.03–6.99 (m, 2H, Ar), 6.21 (s, 2H, Ar), 5.23 (s, 1H, acac), 2.43 (s, 6H, CH_3), 1.79 ppm (s, 6H, CH_3). Anal. calcd. for $C_{53}H_{41}N_4O_2Ir$: C 66.44, H 4.31, N 5.85; found: C 66.32, H 4.43, N 5.98.

7: A bright-yellow powder was obtained in 17% yield. MS (FAB): *m/z* 966 [M^+]. ^{1}H NMR ($CDCl_3$): $\delta = 8.34$ (t, 2H, $J = 5.4$ Hz, Ar), 8.16 (s, 2H, Ar), 7.94--7.86 (m, 4H, Ar), 7.47--7.37 (m, 6H, Ar), 7.31--7.29 (m, 4H, Ar), 7.23--7.09 (m, 6H, Ar), 6.97--6.96 (m, 1H, Ar), 6.54 (s, 1H, Ar), 6.14 (s, 2H, Ar), 5.25 (s, 1H, acac), 1.73 ppm (s, 6H, CH_3). Anal. calcd. for $C_{51}H_{35}N_4F_2O_2Ir$: C 63.41, H 3.65, N 5.80; found: C 63.50, H 3.77, N 5.87.

8: A bright-yellow powder was obtained in 55% yield. MS (FAB): *m/z* 958 (M^+).^{1}H NMR ($CDCl_3$): $\delta = 8.28$ (d, 2H, $J = 2.7$ Hz, Ar), 8.21 (s, 2H, Ar), 7.94 (d, 2H, $J = 5.4$ Hz, Ar), 7.75 (s, 2H, Ar), 7.38--7.09 (m, 15H, Ar), 6.82 (d, 3H, $J = 2.7$ Hz, Ar), 6.16 (s, 2H, Ar), 5.19 (s, 1H, acac), 2.56 ppm (s, 6H, CH_3), 1.76 (s, 6H, CH_3). Anal. calcd. for $C_{53}H_{41}N_4O_2Ir$: C 66.44, H 4.31, N 5.85; found: C 66.29, H 4.40, N 5.99.

X-ray Crystallographic Details

Yellow crystals of **1** that were suitable for X-ray diffraction studies were grown by slow evaporation of its solution in CH_2Cl_2/diethyl ether at room temperature. Geometric and intensity data were collected at 293 K by using graphite-monochromated $Mo_{K\alpha}$ radiation ($\lambda = 0.71073$ Å) on a Bruker Axs SMART 1000 CCD diffractometer. The collected frames were processed with the software SAINT[40] and an absorption correction (SADABS)[41] was applied to the collected reflections. The structure was solved by the Direct methods (SHELXTL)[42] in conjunction with standard difference Fourier techniques and subsequently refined by full-matrix least-squares analyses on F^2. Hydrogen atoms were generated in their idealized positions and all non-hydrogen atoms were assigned with anisotropic displacement parameters. Crystal data for **4**: $C_{72}H_{51}N_6Ir{\cdot}3CH_2Cl_2$, $M_w = 1447.17$, monoclinic, space group $P\bar{1}$, $a = 12.361(1)$, $b = 12.4573(9)$, $c = 22.587(2)$ Å, $\alpha = 104.016(1)$, $\beta = 99.343(1)$, $\gamma = 94.759(2)°$, $V = 3302.5(4)$ Å^3, $Z = 2$, $\rho_{calcd} = 1.455$ Mg m^{-3}, $\mu(Mo_{K\alpha}) = 2.312$ mm^{-1}, $F(000) = 1456$, $T = 293$ K. 16530 reflections measured, of which 11423 were unique ($R_{int} = 0.0332$). Final $R_1 = 0.0447$ and $wR_2 = 0.1138$ for 9266 observed reflections with $I > 2\sigma(I)$. CCDC-687862 contains the supplementary crystallographic data for this paper. These data can be obtained free of charge from The Cambridge Crystallographic Data Centre at www.ccdc.cam.ac.uk/data_request/cif.

OLED Fabrication and Measurements

Commercial ITO-coated glass with sheet resistance of 20–30 Ω/□ was used as the starting substrates. Before device fabrication, the ITO glass substrates were cleaned by ultrasonic baths in organic solvents followed by ozone treatment for 20 min. For device **I**, 40-nm thick NPB film was first deposited on the ITO glass substrates. The phosphor (7%) and CBP host were co-evaporated to form the emitting layer (20 nm). Successively, BCP (8 nm), Alq_3 (20 nm), and Mg:Ag (200 nm) were evaporated. Devices **II–VI** were similarly assembled in the sequence: ITO on glass substrate, 60 nm of NPB, 30 nm of the emitting layer made of CBP host and phosphorescent dopant (x%), 20 nm of BPhen, 1 nm of LiF, and 60 nm of Al. Device **VII** was fabricated as for device **II** but mCP was used as the triplet host. Devices **VIII** and **IX** were constructed in the following sequence: ITO on glass substrate, 40 nm of NPB, 20 nm of the emitting layer made of CBP host and phosphorescent dopant (x%), 10 nm of BCP, 30 nm of Alq_3, and 1:100 nm of LiF/Al co-layer, respectively. The electrical and optical characteristics of these devices were measured by using R6145 DC voltage current source, FLUKE 45 dual display multimeter, Keithley 2400/2000 or Keithley 236 source meter and Spectrascan or PHOTORESEARCH PR650 spectrophotometer in a dark room under ambient air conditions at room temperature. All the measurements finished within 20 min after the device was unloaded from the vacuum chamber.

Acknowledgements

This work was supported by a CERG Grant from the Hong Kong Research Grants Council (HKBU202106) and a Faculty Research Grant from the Hong Kong Baptist University (FRG/04-05/II-59).

[1] a) A. Misra, P. Kumar, M. N. Kamalasanan, S. Chandra, *Semicond. Sci. Technol.* **2006**, *21*, R35–R47; b) B. W. D′Andrade, S. R. Forrest, *Adv. Mater.* **2004**, *16*, 1585–1595.

[2] a) C. W. Tang, S. A. VanSlyke, *Appl. Phys. Lett.* **1987**, *51*, 913–915; b) J. H. Burroughes, D. D. C. Bradley, A. R. Brown, R. N. Marks, K. Mackay, R. H. Friend, P. L. Burns, A. B. Holmes, *Nature* **1990**, *347*, 539–541; c) J. Kido, M. Kimura, K. Nagai, *Science* **1995**, *267*, 1332–1334.

[3] M. A. Baldo, M. E. Thompson, S. R. Forrest, *Nature* **2000**, *403*, 750–753.

[4] a) J. Kido, K. Nagai, Y. Ohashi, *Chem. Lett.* **1990**, 657–660; b) M. A. Baldo, D. F. O'Brien, Y. You, A. Shoustikov, S. Sibley, M. E. Thompson, S. R. Forrest, *Nature* **1998**, *395*, 151–154; c) M. A. Baldo, S. Lamansky, P. E. Burrows, M. E. Thompson, S. R. Forrest, *Appl. Phys. Lett.* **1999**, *75*, 4–6; d) B. Carlson, G. D. Phelan, W. Kaminsky, L. Dalton, X. Jiang, M. S. Liu, A. K.-Y. Jen, *J. Am. Chem. Soc.* **2002**, *124*, 14162–14172; e) S. Bernhard, J. A. Barron, P. L. Houston, H. D. Abruna, J. L. Ruglovksy, X. Gao, G. G. Malliaras, *J. Am. Chem. Soc.* **2002**, *124*, 13624–13628; f) P.-T. Chou, Y. Chi, *Eur. J. Inorg. Chem.* **2006**, 3319–3332; g) R. C. Evans, P. Douglas, C. J. Winscom, *Coord. Chem. Rev.* **2006**, *250*, 2093–2126; h) E. Holder, B. M. W. Langeveld, U. S. Schubert, *Adv. Mater.* **2005**, *17*, 1109–1121; i) P. T. Chou, Y. Chi, *Chem. Soc. Rev.* **2007**, *36*, 1421–1431; j) P.-T. Chou, Y. Chi, *Chem. Eur. J.* **2007**, *13*, 380–395; k) H. Yersin, *Top. Curr. Chem.* **2004**, *241*, 1–26; l) M. A. Baldo, M. E. Thompson, S. R. Forrest, *Pure Appl. Chem.* **1999**, *71*, 2095–2106; m) P. L. Burn, S.-C. Lo, I. D. W. Samuel, *Adv. Mater.* **2007**, *19*, 1675–1688.

[5] a) D. F. O'Brien, M. A. Baldo, M. E. Thompson, S. R. Forrest *Appl. Phys. Lett.* **1999**, *74*, 442–444; b) C. Adachi, M. A. Baldo, S. R. Forrest, S. Lamansky, M. E. Thompson, R. C. Kwong, *Appl. Phys. Lett.* **2001**, *78*, 1622–1624; c) R. J. Holmes, B. W. D′Andrade, S. R. Forrest, X. Ren, J. Li, M. E. Thompson, *Appl. Phys. Lett.* **2003**, *83*, 3818–3820.

[6] a) V. V. Grushin, N. Herron, D. D. LeCloux, W. J. Marshall, A. Petrov, Y. Wang, *Chem. Commun.* **2001**, 1494–1495; b) H. Z. Xie, M. W. Liu, O. Y. Wang, X. H. Zhang, C. S. Lee, L. S. Hung, S. T. Lee, P. F. Teng, H. L. Kwong, H. Zhen, C. M. Che, *Adv. Mater.* **2001**, *13*, 1245–1248; c) J. P. Duan, P. P. Sun, C. H. Cheng, *Adv. Mater.* **2003**, *15*, 224–228; d) T. Tsuzuki, N. Shirasawa, T. Suzuki, S. Tokito, *Adv. Mater.* **2003**, *15*, 1455–1458; e) I. R. Laskar, T. M. Chen, *Chem. Mater.* **2004**, *16*, 111–117; f) C.- J. Chang, C.-H. Yang, K. Chen, Y. Chi, C.-F. Shu, M.- L. Ho, Y.-S. Yeh, P.-T. Chou, *Dalton Trans.* **2007**, 1881–1890; g) G. Zhou, C.- L. Ho, W.-Y. Wong, Q. Wang, D. Ma, L. Wang, Z. Lin, T. B. Marder, A. Beeby, *Adv. Funct. Mater.* **2008**, *18*, 499–511.

[7] A. B. Tamayo, S. Garon, T. Sajoto, P. I. Djurovich, I. M. Tsyba, R. Bau, M. E. Thompson, *Inorg. Chem.* **2005**, *44*, 8723–8732.

[8] a) M. S. Lowry, W. R. Hudson, R. A. Pascal, Jr., S. Bernhard, *J. Am. Chem. Soc.* **2004**, *126*, 14129–14135; b) M. S. Lowry, J. I. Goldsmith, J. D. Slinker, R. Rohl, R. A. Pascal, Jr., G. G. Malliaras, S. Bernhard, *Chem. Mater.* **2005**, *17*, 5712–5719; c) M. S. Lowry, S. Bernhard, *Chem. Eur. J.* **2006**, *12*, 7970–7977; d) F.- M. Hwang, H.-Y. Chen, P.-S. Chen, C.-S. Liu, Y. Chi, C.-F. Shu, F.-I. Wu, P.-T. Chou, S.-M. Peng, G.-H. Lee, *Inorg. Chem.* **2005**, *44*, 1344–1353.

[9] a) S. Lamansky, P. Djurovich, D. Murphy, F. Abdel-Razzaq, R. Kwong, I. Tsyba, M. Bortz, B. Mui, R. Bau, M. E. Thompson, *Inorg. Chem.* **2001**, *40*, 1704–1711; b) S. Lamansky, P. Djurovich, D. Murphy, F. Abdel-Razzaq, H. F. Lee, C. Adachi, P. E. Burrows, S. R. Forrest, M. E. Thompson, *J. Am. Chem. Soc.* **2001**, *123*, 4304–4312; c) M. E. Thompson, S. Lamansky, P. Djurovich, D. Murphy, F. Abdel- Razzaq, R. Kwong, S. R. Forrest, M. A. Baldo, P. E. Burrows, U. S. Patent 20020034656 A1.

[10] a) J. C. Ostrowski, M. R. Robinson, A. J. Heeger, G. C. Bazan, *Chem. Commun.* **2002**, 784–785; b) A. B. Tamayo, B. D. Alleyne, P. Djurovich, S. Lamansky, I. Tsyba, N. N. Ho, R. Bau, M. E. Thompson, *J. Am. Chem. Soc.* **2003**, *125*, 7377–7387; c) C. H. Yang, K. H. Fang, C. H. Chen, I. W. Sun, *Chem. Commun.* **2004**, 2232–2233; d) J. Nishida, H. Echizen, T. Iwata, Y. Yamashita, *Chem. Lett.* **2005**, *34*, 1378–1379; e) C. S. K. Mak, A. Hayer, S. I. Pascu, S. E. Watkins, A. B. Holmes, A. Köhler, R. H. Friend, *Chem. Commun.* **2005**, 4708–4710; f) S. Bettington, M. Tavasli, M. R. Bryce, A. S. Batsanov, A. L. Thompson, H. A. A. Attar, F. B. Dias, A. P. Monkman, *J. Mater. Chem.* **2006**, *16*, 1046–1052.

[11] a) C. Adachi, R. C. Kwong, P. Djurovich, V. Adamovich, M. A. Baldo, M. E. Thompson, S. R. Forrest, *Appl. Phys. Lett.* **2001**, *79*, 2082–2084; b) S. Tokito, T. Iijima, Y. Suzuri, H. Kita, T. Tsuzuki, F. Sato, *Appl. Phys. Lett.* **2003**, *83*, 569–571; c) S. J. Yeh, M. F. Wu, C. T. Chen, Y. H. Song, Y. Chi, M. H. Ho, S. F. Hsu, C. H. Chen, *Adv. Mater.* **2005**, *17*, 285–289; d) P. Coppo, E. A. Plummer, L. De Cola, *Chem. Commun.* **2004**, 1774–1775; e) R. Ragni, E. A. Plummer, K. Brunner, J. W. Hofstraat, F. Babudri, G. M. Farinola, F. Naso, L. De Cola, *J. Mater. Chem.* **2006**, *16*, 1161–1170; f) S. Takizawa, H. Echizen, J. Nishida, T. Tsuzuki, S. Tokito, Y. Yamashita, *Chem. Lett.* **2006**, *35*, 748–749; g) C.-H. Yang, Y.- M. Cheng, Y. Chi. C.- J. Hsu, F.-C. Fang, K.-T. Wong, P.-T. Chou, C.-H. Chang, M.-H. Tsai, C.-C. Wu, *Angew. Chem.* **2007**, *119*, 2470–2473; *Angew. Chem. Int. Ed.* **2007**, *46*, 2418–2421.

[12] a) S. Bettington, M. Tavasli, M. R. Bryce, A. Beeby, H. Al-Attar, A. P. Monkman, *Chem. Eur. J.* **2007**, *13*, 1423–1428; b) C.- L. Li, Y.-J. Su, Y.-T. Tao, P.-T. Chou, C.-H. Chien, C.-C. Cheng, R.-S. Liu, *Adv. Funct. Mater.* **2005**, *15*, 387–395; c) S.-Y. Chang, J. Kavitha, J.-Y. Hung, Y. Chi, Y.- M. Cheng, E. Y. Li, P.-T. Chou, G.-H. Lee, A. J. Carty, *Inorg. Chem.* **2007**, *46*, 7064–7074.

[13] a) W. Y. Wong, C. L. Ho, Z. Q. Gao, B. X. Mi, C. H. Chen, K. W. Cheah, Z. Lin, *Angew. Chem.* **2006**, *118*, 7964–7967; *Angew. Chem. Int. Ed.* **2006**, *45*, 7800–7803; b) C. L. Ho, M. F. Lin, W. Y. Wong, W. K. Wong, C. H. Chen, *Appl. Phys. Lett.* **2008**, *92*, 083301-1–083301-3; c) C. L. Ho, W. Y. Wong, Z. Q. Gao, C. H. Chen, K. W. Cheah, B. Yao, Z. Xie, Q. Wang, D. Ma, L. Wang, X. M. Yu, H. S. Kwok, Z. Lin, *Adv. Funct. Mater.* **2008**, *18*, 319–331; d) C. L. Ho, W. Y. Wong, G. J. Zhou, B. Yao, Z. Xie, L. Wang, *Adv. Funct. Mater.* **2007**, *17*, 2925–2936; e) C. L. Ho, W. Y. Wong, Q. Wang, D. Ma, L. Wang, Z. Lin, *Adv. Funct. Mater.* **2008**, *18*, 928–937; f) Y.-H. Sun, X.-H. Zhu, Z. Chen, Y. Zhang, Y. Cao, *J. Org. Chem.* **2006**, *71*, 6281–6284; g) C. Yang, X. Zhang, H. You, L. Zhu, L. Chen, L. Zhu, Y. Tao, D. Ma, Z. Shuai, J. Qin, *Adv. Funct. Mater.* **2007**, *17*, 651–661; h) J. Ding, J. Gao, Y. Cheng, Z. Xie, L. Wang, D. Ma, X. Jing, F. Wang, *Adv. Funct. Mater.* **2006**, *16*, 575–581; i) G.- J. Zhou, C.- L. Ho, W.-Y. Wong, Q. Wang, D. Ma, L. Wang, Z. Lin, *Chem. Asian J.* **2008**, doi:10.1002/asia.200800074.

[14] a) K. Brunner, A. van Dijken, H. Börner, J. J. A. M. Bastiaansen, N. M. M. Kiggen, B. M. W. Langeveld, *J. Am. Chem. Soc.* **2004**, *126*, 6035–6042; b) O. Paliulis, J. Ostrauskaite, V. Gaidelis, V. Jankauskas, P. Strohriegl, *Macromol. Chem. Phys.* **2003**, *204*, 1706–1712; c) M. K. Nazeeruddin, R. Humphry-Baker, D. Berner, S. Rivier, L. Zuppiroli, M. Graetzel, *J. Am. Chem. Soc.* **2003**, *125*, 8790–8797; d) C. Adachi, M. A. Baldo, M. E. Thompson, S. R. Forrest, *Appl. Phys. Lett.* **2001**, *90*, 5048–5051; e) C.-T. Chen, *Chem. Mater.* **2004**, *16*, 4389–4400; f) K. R. Kustin Thomas, J. T. Lin, Y.-T. Tao, C.-W. Ko, *J. Am. Chem. Soc.* **2001**, *123*, 9404–9411; g) W. Y. Wong, *Coord. Chem. Rev.* **2005**, *249*, 971–997.

[15] K. Dedeian, P. I. Djurovich, F. O. Garces, G. Carlson, R. J. Watts, *Inorg. Chem.* **1991**, *30*, 1685–1687.

[16] M. G. Colombo, T. C. Brunold, T. Riedener, H. U. Güdel, M. Förtsch, H. Bürgi, *Inorg. Chem.* **1994**, *33*, 545–550.

[17] F. O. Garces, K. Dedian, N. L. Keder, R. J. Watts, *Acta Crystallogr. Sect. C* **1993**, *49*, 1117–1120.

[18] Y. Wang, N. Herron, V. V. Grushin, D. LeCloux, V. Petrov, *Appl. Phys. Lett.* **2001**, *79*, 449–451.

[19] a) S. Jung, Y. Kang, H.-S. Kim, Y.-H. Kim, C.-L. Lee, J.-J. Kim, S.-K. Lee, S.-K. Kwon, *Eur. J. Inorg. Chem.* **2004**, 3415–3423; b) M. G. Colombo, A. Hauser, H. U. Gudel, *Inorg. Chem.* **1993**, *32*, 3088–3092; c) D. K. Rayabarapu, B. M. J. S. Paulose, J.-P. Duan, C.-H. Cheng, *Adv. Mater.* **2005**, *17*, 349–353; d) Y. H. Song, S.-J. Yeh, C.-T. Chen, Y. Chi, C.-S. Liu, J.-K. Yu, Y.-H. Hu, P.-T. Chou, S.-M. Peng, G.-H. Lee, *Adv. Funct. Mater.* **2004**, *14*, 1221–1226; e) T. D. Anthopoulos, M. J. Frampton, E. B. Namdas, P. L. Burn, I. D. W. Samuel, *Adv. Mater.* **2004**, *16*, 557–560; f) Y.-J. Su, H.-L. Huang, C.-L. Li, C.-H. Chien, Y.-T. Tao, P.-T. Chou, S. Datta, R.-S. Liu, *Adv. Mater.* **2003**, *15*, 884–888; g) K. R. Justin Thomas, M. Velusamy, J. T. Lin, C.-H. Chien, Y.-T. Tao, Y. S. Wen, Y.-H. Hu, P.-T. Chou, *Inorg. Chem.* **2005**, *44*, 5677–5685; h) W.-S. Huang, J.-T. Lin, C.-H. Chien, Y.-T. Tao, S.-S. Sun, Y.-S. Wen, *Chem. Mater.* **2004**, *16*, 2480–2488; i) S. Okada, K. Okinaka, H. Iwawaki, M. Furugori, M. Hashimoto, T. Mukaide, J. Kamatani, S. Igawa, A. Tsuboyama, T. Takiguchi, K. Ueno, *Dalton Trans.* **2005**, 1583–1590.

[20] P. J. Hay, *J. Phys. Chem. A* **2002**, *106*, 1634–1641.

[21] J. Brooks, T. Babaya, S. Lamansky, P. I. Djurovich, I. Tsyba, R. Bau, M. E. Thompson, *Inorg. Chem.* **2002**, *41*, 3055–3066.

[22] P. J. Spellane, R. J. Watts, *Inorg. Chem.* **1993**, *32*, 5633–5636.

[23] F. O. Garces, K. A. King, R. J. Watts, *Inorg. Chem.* **1988**, *27*, 3464–3471.

[24] A. Tsuboyama, H. Iwawaki, M. Furugori, T. Mukaide, J. Kamatani, S. Igawa, T. Moriyama, S. Miura, T. Takiguchi, S. Okada, M. Hoshino, K. J. Ueno, *J. Am. Chem. Soc.* **2003**, *125*, 12971–12979.

[25] a) S. D. Cummings, R. Eisenberg, *J. Am. Chem. Soc.* **1996**, *118*, 1949–1960; b) N. J. Demas, G. A. Crosby, *J. Am. Chem. Soc.* **1970**, *92*, 7262–7270; c) A. C. Spivey, D. J. Turner, S. Yeates, *Org. Lett.* **2002**, *4*, 1899–1902; d) J. L. Bréfort, R. J. P. Corriu, P. Gerbier, C. Guérin, B. J. L. Henner, A. Jean, T. Kuhlmann, F. Garnier, A. Yassar, *Organometallics* **1992**, *11*, 2500–2506.

[26] M. K. Nazeeruddin, R. T. Wegh, Z. Zhou, C. Klein, Q. Wang, F. De Angelis, S. Fantacci, M. Gratzel, *Inorg. Chem.* **2006**, *45*, 9245–9250.

[27] H. Jang, C. H. Shin, N. G. Kim, K. Y. Hwang, Y. Do, *Synth. Met.* **2005**, *154*, 157–160.

[28] Y. H. Park, Y. S. Kim, *Curr. Appl. Phys.* **2007**, *7*, 500–503.

[29] B. W. D′Andrade, M. A. Baldo, C. Adachi, J. Brooks, M. E. Thompson, S. R. Forrest, *Appl. Phys. Lett.* **2001**, *79*, 1045–1047.

[30] C. W. Ko, Y. T. Tao, J. T. Lin, K. R. Justin Thomas, *Chem. Mater.* **2002**, *14*, 357–361.

[31] G. He, M. Pfeiffer, K. Leo, M. Hofmann, J. Birnstock, R. Pudzich, J. Salbeck, *Appl. Phys. Lett.* **2004**, *85*, 3911–3913.

[32] L. S. Sapochak, A. Padmaperuma, N. Washton, F. R. Endrino, G. T. Schmett, J. Marshall, D. Fogarty, P. E. Burrows, S. R. Forrest, *J. Am. Chem. Soc.* **2001**, *123*, 6300–6307.

[33] M. A. Baldo, C. Adachi, S. R. Forrest, *Phys. Rev. B* **2000**, *62*, 10967–10977.

[34] J. Kalinowski, W. Stampor, J. Mezyk, M. Cocchi, D. Virgili, V. Fattori, P. Di Marco, *Phys. Rev. B* **2002**, *66*, 235321–1.

[35] M. A. Baldo, S. R. Forrest, *Phys. Rev. B* **2000**, *62*, 10958–10966.

[36] a) F. Barigelletti, D. Sandrini, M. Maestri, V. Balzani, A. von Zelewsky, L. Chassot, P. Jolliet, U. Maeder, *Inorg. Chem.* **1988**, *27*, 3644–3647; b) K. Naito, A. Miura, *J. Phys. Chem.* **1993**, *97*, 6240–6248; c) M.-F. Wu, S.- J. Yeh, C.-T. Chen, H. Murayama, T. Tsaboi, W.-S.

Li, I. Chao, S.-W. Liu, J.- K. Wang, *Adv. Funct. Mater.* **2007**, *17*, 1887–1895.
[37] a) L. Liu, W.-Y. Wong, J.-X. Shi, K.-W. Cheah, *J. Polym. Sci. Part A: Polym. Chem.* **2006**, *44*, 5588–5607; b) L. Liu, W.-Y. Wong, J.-X. Shi, K.-W. Cheah, T.-H. Lee, L. M. Leung, *J. Organomet. Chem.* **2006**, *691*, 4028–4041.
[38] a) W. R. Wadt, P. J. Hay, *J. Chem. Phys.* **1985**, *82*, 284–298; b) P. J. Hay, W. R. Wadt, *J. Chem. Phys.* **1985**, *82*, 299–310.
[39] G. Schaftenaar, *Molden* v3.7; CAOS/CAMM Center Nijmegen: Toernooiveld, Nijmegen, Netherlands, **2001**.
[40] SAINT+, ver. 6.02a, Bruker Analytical X-ray System, Inc., Madison, WI, **1998**.
[41] G. M. Sheldrick, SADABS, Empirical Absorption Correction Program; University of Göttingen, Germany, **1997**.
[42] G. M. Sheldrick, SHELXTL™, Reference manual, ver. 5.1, Madison, WI, **1997**.

Received: June 3, 2008
Published online: October 10, 2008

